



**Repositorio Institucional de la Universidad Autónoma de Madrid**

<https://repositorio.uam.es>

Esta es la **versión de autor** del artículo publicado en:

This is an **author produced version** of a paper published in:

Journal of Comparative Neurology 524.15 (2016): 3084-3103

**DOI:** <http://dx.doi.org/10.1002/cne.24010>

**Copyright:** © 2016 Wiley Periodicals

El acceso a la versión del editor puede requerir la suscripción del recurso

Access to the published version may require subscription

# **Electron Microscopic Localization of M2-muscarinic receptors in Cholinergic and Non-Cholinergic Neurons of the Laterodorsal Tegmental and Pedunculo pontine Nuclei of the Rat Mesopontine Tegmentum**

**Miguel Garzón<sup>1,2,3\*</sup> and Virginia M. Pickel<sup>3</sup>**

<sup>1</sup>Departamento de Anatomía, Histología y Neurociencia, Facultad de Medicina UAM, Madrid, 28029, Spain, <sup>2</sup>Instituto de Investigación Hospital Universitario La Paz (IDIPAZ), Paseo de la Castellana 261, Madrid 28046, Spain, <sup>3</sup>Department of Neuroscience, Brain and Mind Research Institute, Weill Cornell Medical College, 407 East 61st Street, New York, NY 10065, USA.

**Number of text pages:** 58

**Number of figures:** 6

**Number of tables:** 3

**Running title:** M2 activation sites in PPT/LDT neurons

**Associate Editor to whom this manuscript is also submitted:** Dr. Oswald Steward

**Keywords:** vesicular acetylcholine transporter, acetylcholine, autoreceptor, sleep-wake, reward, AB\_2039995, AB\_572269.

\*Correspondence to: Dr. Miguel Garzón  
Department of Anatomy, Histology and Neuroscience  
Medical School UAM  
Arzobispo Morcillo 4  
28029 Madrid  
Tel: (34) 91-497-5466  
Fax: (34) 91-497-5353  
Email: miguel.garzon@uam.es

This work was supported with Grants from MECD (PRX14/00530) and MINECO (BFU2013-43741-P) to M.G. and NIH/NIMH (MH40342), NIH (HL09657) and NIDA (DA04600 and DA005130) to V.M.P.

**ABSTRACT**

Muscarinic m2 receptors (M2Rs) are implicated in autoregulatory control of cholinergic output neurons located within the pedunculo pontine (PPT) and laterodorsal tegmental (LTD) nuclei of the mesopontine tegmentum (MPT). However, these nuclei contain many non-cholinergic neurons in which activation of M2R heteroceptors may contribute significantly to the decisive role of the LTD and PPT in sleep-wakefulness. We examined the electron microscopic dual immunolabeling of M2Rs and the vesicular acetylcholine transporter (VAChT) in the MPT of rat brain to identify the potential sites for M2R activation. M2R immunogold labeling was predominately seen in somatodendritic profiles throughout the PPT/LTD complex. In somata, M2R immunogold particles were often associated with Golgi lamellae and cytoplasmic endomembranes, but were rarely in contact with the plasma membrane as was commonly seen in dendrites. Approximately 36% of the M2R-labeled somata and 16% of the more numerous M2R-labeled dendrites co-expressed VAChT. M2R and M2R/VAChT-labeled dendritic profiles received synapses from inhibitory- and excitatory-type axon terminals, over 88% of which were unlabeled and others contained exclusively M2R or VAChT immunoreactivity. In axonal profiles M2R immunogold was localized to plasmalemmal and cytoplasmic regions and showed a similar distribution in many VAChT-negative glial profiles. These results provide ultrastructural evidence suggestive of somatic endomembrane trafficking of M2Rs, whose activation serves to regulate the postsynaptic excitatory and inhibitory responses in dendrites of cholinergic and non-cholinergic neurons in the MPT. They also suggest the possibility that M2Rs in this brain region mediate the effects of acetylcholine on the release of other neurotransmitters and on glial signaling.

## INTRODUCTION

Acetylcholine (ACh) is highly implicated in cortical activation both in wakefulness and in REM sleep (Jones, 1993), but also plays a role in the appearance of some specific REM sleep state characteristic features such as muscle atonia or PGO waves (Moreno-Balandrán et al., 2008). Many of the cholinergic neurons that are most involved in these complex processes are distributed in Ch5 and Ch6 cell groups respectively located in the pedunculopontine (PPT) and laterodorsal tegmental (LDT) nuclei and their boundaries within the mesopontine tegmentum (MPT). Axons of these cholinergic neurons are part of the reticular activating system that widely innervates the cerebral cortex through thalamic relay or even direct connections (Cornwall et al., 1990; Jones, 1993; Cid-Pellitero and Garzón, 2011). Injection of cholinergic agonists in portions of the pontine reticular formation that receives input from neurons in the PPT/LDT provokes a pharmacologically-induced REM-like state resembling natural REM sleep in cats (for review see Reinoso-Suárez et al., 2001) and rats (Gnadt and Pegram, 1986; Horner and Kubin, 1999). During the cholinergically-evoked REM-like state ACh release is increased in the oral pontine reticular formation (Lydic et al., 1991) paralleling what happens in natural REM (Kodama et al., 1990) or after MPT electrical stimulation (Lydic and Baghdoyan, 1993). Furthermore, MPT cholinergic neurons defined by their content of the vesicular acetylcholine transporter (VAChT) discharge in association with evoked cortical activation in anesthetized rats (Boucetta and Jones, 2009), and discharge maximally during wakefulness and REM sleep in naturally-sleeping rats (Boucetta et al., 2014). The expression of the immediate early gene, *c-fos*, is also increased in cholinergic neurons in the PPT/LDT during the (1) ACh-induced REM-like state (Shiromani et al., 1996), and (2) REM sleep rebound period following REM sleep deprivation (Maloney et al., 1999).

Involvement of muscarinic ACh receptors in the REM sleep elicitation by PPT/LDT cholinergic neurons is evidenced by the effective blocking of both natural and

cholinergically-evoked REM sleep by microinfusion of the muscarinic antagonist, atropine, in the oral pontine reticular formation (Shiromani and Fishbein, 1986; Baghdoyan et al., 1989). The output of MPT cholinergic neurons to the reticular formation or the midbrain is thought to be tightly autoregulated by muscarinic inhibitory autoreceptors in their cell bodies or dendrites. Muscarinic agonists strongly hyperpolarize while antagonists depolarize MPT cholinergic neurons, thus increasing their output to targets within the reticular formation (Luebke et al., 1993; Leonard and Llinás, 1994) and Ach release (Roth et al., 1996; Chen et al., 2006). Likewise, infusion of the muscarinic antagonist scopolamine in the PPT/LDT increases dopamine midbrain neuron activity, dopamine-related behaviors and striatal dopamine release (Chapman et al., 1997; Miller and Blaha, 2004; Lodge and Grace, 2006; Di Giovanni and Shi, 2009). These effects are comparable to those produced by pharmacological stimulation of cholinergic receptors in dopaminergic neurons in substantia nigra or ventral tegmental area (VTA) (Blaha and Winn, 1993; Blaha et al., 1996).

The muscarinic receptor family is comprised of five cloned G protein-coupled receptors with seven transmembrane domains (M1-M5) (Kubo et al., 1986; Bonner et al., 1987, 1988; Peralta et al., 1987). These can be classified into two major functional groups according to their G-protein coupling affinity: M1, M3 and M5 receptors selectively couple to  $G_q$  proteins and stimulate inositol phosphate pathways, whereas M2 and M4 receptors have selectivity for  $G_{i/o}$  proteins and inhibit adenylyl cyclase activity (Wess et al., 1996). These latter receptor subtypes represent the main inhibitory muscarinic autoreceptors in the brain, as M2/M4  $G_{\alpha i}$  protein-mediated signaling in many brain regions produce hyperpolarization at postsynaptic sites (Luebke et al., 1993; Leonard and Llinás, 1994; Calabresi et al., 1998) and/or presynaptic inhibition of neurotransmitter release from axon terminals (Billard et al., 1995; Zhang et al., 2002).

Muscarinic receptor family members have been identified by (1) *in situ* hybridization for their mRNAs (Buckley et al., 1988; Weiner et al., 1990; Vilaró et al.,

1992, 1994), and (2) *in vitro* receptor autoradiographic detection of labeled radioligands in the brainstem of rodents and cats (Frey and Howland, 1992; Baghdoyan et al., 1994). The M2 receptor subtype (M2R) was found to be the predominant muscarinic receptor in the brainstem of both species (Vilaró et al., 1992, 1994; Baghdoyan, 1997). Earlier studies have also specifically implicated the M2R in muscarinic hyperpolarization of cholinergic neurons in the MPT (Luebke et al., 1993; Leonard and Llinás, 1994). This has been confirmed by the reduced muscarinic hyperpolarization of MPT neurons produced by administration of selective M2R antagonists (Ye et al., 2010) or by M2R gene deletion in mice (Kohlmeier et al., 2012). However, there is also substantial evidence for a heteroreceptor function of M2Rs in many brain regions (Rouse et al., 2000; Bernard et al., 1998; Garzón and Pickel, 2006). Thus, M2Rs may also play a critical role as cholinergic autoreceptors and heteroreceptors within the MPT (Garzón and Pickel, 2000). This possibility was suggested previously by the demonstration of M2Rs in cholinergic and non-cholinergic neurons in the LDT (Kohlmeier et al., 2012). However, it is not known whether M2Rs in either the PPT or LDT are preferentially located near the sites for Ach storage and release as revealed by the expression of the VAChT. To address this important question, we used electron microscopy immunocytochemistry for dual labeling of M2R and VAChT in PPT and LDT of rat brain. The results provide the first ultrastructural evidence that VAChT and M2R have partially overlapping and segregated distributions in many somata and dendrites, and an almost completely segregated distribution in axonal and glial processes throughout the PPT/LDT complex.

## MATERIAL AND METHODS

### Antibody characterization

A goat polyclonal antiserum raised against a C terminal synthetic peptide sequence corresponding to amino acids 511-530 as predicted from the cloned rat VAChT (Erickson et al., 1994; Roghani et al., 1994) was obtained (ref. 24286, RRID: AB\_572269) from ImmunoStar (Hudson, WI) (Table 1). This peptidic fragment shows a remarkable similarity with its human counterpart (85%, Varoqui et al., 1996), and has no sequence homology with other vesicular transporter family members (Bejanin et al., 1994). The VAChT antiserum is well characterized and has been used previously in ultrastructural dual-labeling studies in the MPT and many other brain regions (Garzón et al., 1999, 2000; Pickel et al., 2000; Muller et al., 2013). This antiserum has been shown to recognize the VAChT protein, but not related vesicular monoamine transporter-2 protein, in cells transfected with the correspondent cDNAs (Arvidsson et al., 1997). The selectivity of the VAChT antiserum used in the present study is supported by the distributional and morphological similarity between the VAChT-immunolabeled neurons and neurons expressing VAChT mRNA (Butcher et al., 1992; Roghani et al., 1996). The VAChT antiserum used in our study also labels selectively cells that are known to express VAChT, such as PC 12 cells and spinal motoneurons in primary culture (Arvidsson et al., 1997). The immunolabeling was further shown to be specific for the antigenic VAChT peptide by absence of immunoreactivity in sections of brain tissue processed for immunolabeling after prior adsorption with cognate peptide but not with the carrier protein (Arvidsson et al., 1997).

The M2R immunoreactivity was detected with a rabbit polyclonal antiserum (product number AMR-002, Lot AN-08, RRID: AB\_2039995, Alomone Labs Ltd, Jerusalem, Israel) (Table 1). This antiserum was directed against a synthetic fusion protein containing Glutathione S-transferase fused to a part of the i3 intracellular loop of human M2R (residues 225-356) (Bonner et al., 1987; Peralta et al., 1987; Levey et al., 1991). The identity of the fusion protein was confirmed by DNA sequence and SDS-PAGE Western blotting of rat brain membranes. The specificity of the M2R antiserum

has been previously verified by loss of immunoreactivity in brain tissue processed using preadsorbed antisera in wild-type, or unadsorbed M2R antisera M2R knockout mice (Garzón et al., 2006). In the present study, we established the absence of labeling for VAChT in the rat MPT after prior adsorption of the M2R antiserum with excess immunogen fusion protein (3 µg/mg) (product number AMR-002, Lot AN-08, Alomone Labs Ltd, Jerusalem, Israel). The pattern of labeling seen using the M2R antiserum in the present study was similar to that previously observed with other antibodies against M2R in the MPT (Brischoux et al., 2008; Kohlmeier et al., 2012) and known M2R mRNA localization (Weiner et al., 1990; Vilaró et al., 1992, 1994). This pattern was also unaffected by switching the immunogold and immunoperoxidase markers or by suppressing the secondary antibody incubation step when using the VAChT and M2R antisera.

### **Tissue preparation**

Four (250-300 g) male Sprague-Dawley rats (Taconic, Germantown, NY) were deeply anesthetized with 100 mg/kg i.p. sodium pentobarbital in preparation of their brain tissue for immunolabeling as described initially by Lanthorn and Pickel (1989). All efforts were made to minimize animal suffering, and to use the minimal necessary number of animals. The experimental protocol strictly conformed with National Institutes of Health guidelines for the Care and Use of Laboratory Animals and was approved by the Institutional Animal Care and Use Committee of the Weill Medical College of Cornell University.

The anesthetized rats were subject to sequential aortic arch perfusion with (1) 20 ml of heparin (1000 U/ml) in saline, (2) 50 ml of 3.8% acrolein (Polysciences, Warrington, PA) in a solution of 2% paraformaldehyde in 0.1 M phosphate buffer (PB), and (3) 200 ml of 2% paraformaldehyde in 0.1 M PB. The aldehyde-fixed brains were removed from the cranium, dissected and postfixed for 30 minutes in 2%



paraformaldehyde. Coronal sections through the MPT were cut at 40-50  $\mu\text{m}$  thickness using a Leica Vibratome VT1000 S (Leica Instruments GmbH, Nussloch, Germany). These sections were placed in 0.1 M PB at 4°C, then incubated for 30 minutes in a solution of 1% sodium borohydride in 0.1 M PB to remove excess of active aldehydes. To enhance the penetration of immunoreagents, the sections were then cryoprotected for 15 minutes in a solution of 25% sucrose and 3% glycerol in 0.05 M PB, frozen quickly in liquid chlorodifluoromethane (Freon; Refron Inc., NY) followed by liquid nitrogen, and thawed in 0.1 M PB at room temperature. After extensive rinsing in 0.1 M Tris-buffered saline (TS), the sections were incubated for 30 minutes in 0.5% bovine serum albumin (BSA) in 0.1 M TS to minimize detection of nonspecific labeling.

### Dual immunocytochemical labeling

Tissue sections through the MPT were processed for combined immunoperoxidase and immunogold-silver labeling of VAChT and M2R prior to plastic embedding using a pre-embedding method described by Chan et al. (1990). Thus, the immunoperoxidase reaction for VAChT was followed by immunogold-silver detection of M2R, since the immunogold method gives a more precise subcellular localization of the receptors than the immunoperoxidase method. The primary antisera against VAChT and M2R were raised in goats and rabbits respectively, and therefore could be recognized by appropriate species-specific secondary antibodies. All the incubations during the procedure, save for the primary antisera, were carried out at room temperature. They occurred with continuous agitation on a rotary shaker and were followed by several rinses in 0.1 M TS, 0.1 M PB and 0.01 M phosphate-buffered saline (PBS).

Tissue sections from four rats were incubated for 36-42 hours at 4°C in a cocktail solution containing 1:16000 goat anti-VAChT and 1:100 rabbit anti-M2R antisera. For the immunoperoxidase visualization of VAChT, we used the avidin-biotin complex

(ABC) method (Hsu et al., 1981). Briefly, following the incubation in primary antisera, the sections were incubated in secondary biotinylated donkey anti-goat IgG (1:400, Jackson ImmunoResearch, West Grove, PA) for 30 minutes and then in ABC (1:100, Vectastain Elite Kit, Vector Laboratories, Burlingame, CA) for another 30 minutes. The VAChT immunoreactivity was visualized by a 6 minute incubation in a solution containing 0.022% 3,3'-diaminobenzidine and 0.003% hydrogen peroxide in 0.1 M TS.

After the peroxidase reaction, the sections were washed in 0.1 M TS, transferred to 0.01 M PBS, blocked for 10 minutes in 0.8% BSA and 0.1% gelatin in 0.01 M PBS, and incubated for 2 hours in colloidal gold (0.8 nm)-labeled donkey anti- rabbit IgG (1:50; Electron Microscopy Sciences, Hatfield, PA). After this, the sections were rinsed in 0.01 M PBS first with then without the addition of BSA and gelatin. They were next placed for 10 minutes in 2% glutaraldehyde in 0.01 M PBS to secure the bound gold particles in the tissue. These sections were then reacted with a silver enhancement solution IntenSEM kit (Amersham, Arlington Heights, IL) for either (1) 5-8 minutes for electron microscopy, or (2) 10-12 minutes for light microscopy. Sections processed for light microscopy were rinsed in 0.05 M PB and mounted on glass slides. After overnight drying in a dessicator, they were dehydrated through immersion in a series of increasing-concentration alcohols, and defatted in a series of xylenes (J.T. Baker, Phillipsburg, NJ). Finally, the slides were coverslipped and examined in a Nikon microscope using differential interference contrast optics. A few sections in both PPT and LDT were reacted using a reversal of markers (M2R immunoperoxidase, antibody dillution: 1:2000 and VAChT immunogold, antibody dillution: 1:3000) in order to verify the reliability of labeling regardless the immunohistochemical method and thus avoid bias in labeling.

### **Electron microscopy**

Immunolabeled sections for electron microscopy were rinsed in 0.1 M PB, postfixed in 2% osmium tetroxide in 0.1 M PB for 1 hour, dehydrated through a series of graded ethanols and propylene oxide, and placed overnight in a 1:1 mixture of propylene oxide and Epon resin (EM bed-812; Electron Microscopy Sciences, Fort Washington, PA). The next day the sections were transferred to 100% Epon for 2 hours and flat-embedded in Epon between two sheets of Aclar plastic film (Allied Signal, Pottsville, PA). Flat-embedded sections were then allowed to harden in an oven for 64 hr at 58-60°C. The tissue areas of interest within the MTP were identified and selected using a light microscope. Excised embedded tissue was glued to a plastic block and trimmed to trapezoidal surface pyramids. Ultrathin sections (40-50 nm) were cut from the outer surface of the tissue in the plastic-tissue interface with a diamond knife (Diatome, Fort Washington, PA) by using an ultramicrotome (Ultratome, NOVA; LKB-Product AB, Bromma, Sweden). The regions examined were located in the PPT and the LDT at the levels of anteroposterior plane -8.30 mm from Bregma of the rat brain atlas of Swanson (1992). The sections were collected and dried on copper mesh grids, then counterstained with uranyl acetate and lead citrate (Reynolds, 1963). They were analyzed and photographed using a Tecnai Biotwin 12 (Serial # D271) electron microscope (FEI Company, Hillsboro, OR).

### **Data analysis**

Only sections near the surface of the tissue at the Epon-tissue interface where penetration of the antisera and immunoreagents is optimal were examined in order to reduce false negatives and to ensure that both markers were detectable in all sections used for analysis. However, we may have still underestimated the presence of immunolabeled profiles in the immunogold-processed tissue due to the sparse discrete subcellular distribution of gold particles, especially within small profiles such as the axonal and glial profiles that were found to be less numerous than larger

somatodendritic structures. This potential inconvenience was partially overcome by using as well the ABC method that, although having a more limited resolution for subcellular localization, possess a higher sensitivity for detection of small immunoreactive profiles. These precautions greatly enhanced the method reliability and indicate that the prevalence of interactions between the two antigens - coexpression or synaptic contacts- are at least as large and probably larger than those reported in the results section.

The classification of identified cellular elements was based on the descriptions of Peters et al. (1991). Axon terminals were identified by the presence of numerous synaptic vesicles and were at least 0.2  $\mu\text{m}$  in diameter. Small unmyelinated axons were <0.2  $\mu\text{m}$  and rarely contained small vesicles. Neuronal somata were identified by the presence of a nucleus, and a perinuclear cytoplasm containing an abundance of organelles. Dendrites usually contained abundant endoplasmic reticulum, and were distinguished from unmyelinated axons by their larger diameter and/or abundance of uniformly distributed microtubules. Most dendritic profiles were also postsynaptic to axon terminals. Asymmetric synapses were identified by thick postsynaptic densities, while symmetric synapses had thin pre- and post-synaptic specializations (Gray, 1959). Zones of closely spaced parallel plasma membranes, which lacked recognizable synaptic densities, but were otherwise not separated by glial processes, were defined as appositions or nonsynaptic contacts, and were not included in the quantification. Astrocytic processes were defined by their irregular contour, vacuous cytoplasm and sporadic presence of intermediate filaments. Labeled small-diameter profiles without recognizable morphology of dendritic, axonal, or glial processes were simply called processes.

VAChT-immunoperoxidase labeled profiles were defined by their content of electron dense precipitate that was not seen in other morphologically similar profiles in the surrounding neuropil. A profile was considered to contain immunogold labeling

when two or more gold particles were observed within large profiles or when a single particle was seen in small profiles, such as unmyelinated small axons. This approach has been shown to be valid when there is (1) minimal labeling of tissue not known to express M2R, such as myelin sheaths, and (2) little if any spurious distribution of gold–silver deposits at the tissue/epon interface (Garzón et al., 2006). These criterion were met in the present study, so the quantitative analysis was not corrected for background labeling.

The ultrastructural analysis was carried out in 18 vibratome sections (11 were cut through the PPT and the other 7 through the LDT) that were obtained from four animals, each animal contributing at least 4 sections. All immunoreactive processes ( $n=2874$ ) were counted in randomly sampled electron micrographs at magnifications of 9,300–30,000 X from an area of  $25,487 \mu\text{m}^2$  ( $15,123 \mu\text{m}^2$  within the PPT and  $10,364 \mu\text{m}^2$  within the LDT) with an area of at least  $2,693 \mu\text{m}^2$  (PPT) and  $1,660 \mu\text{m}^2$  (LDT) examined in each animal. The tissue was quantitatively examined to determine the relative frequencies with which the immunoreactive products were localized within neuronal somata, dendrites, axons or glial cells. In addition, morphologically recognizable synaptic junctions of each labeled profile were also quantified. Nested ANOVAs were used to determine whether there was significant variability in total labeled profiles per square micron of analyzed surface with respect to (1) different animals, (2) cholinergic MPT subdivisions (LDT vs PPT) or (3) immunocytochemical method. Post-hoc comparisons between pairs were done using Fisher's exact test. Variations in the density (mean number per cross-sectional surface unit) of asymmetric and symmetric synapses established by either M2R-immunolabeled terminals or M2R-immunoreactive dendrites were assessed using Student t-tests.

An analysis of the ultrastructural distribution of M2R was carried out to ascertain (1) the prevalence of M2R in association with specific cellular structures and (2) the relationship between M2R- and VAChT-immunolabeled profiles. The prevalence of

different profile types (i.e., dendrites vs axons, etc.) containing M2R was expressed as a percentage of all M2R-labeled elements. These M2R-labeled profiles were assessed from four to five vibratome sections from each of four animals (n=18). The tissue was also used for the examination of the relative number of gold–silver particles in association with either the plasma membrane or the cytoplasm of the M2R-immunogold labeled dendrites and axon terminals. A particle was considered to be associated to the plasma membrane when any point of its contour was in contact with the plasma membrane. Assessment of the immunogold distribution of M2R was based on 4711 gold–silver particles within 1345 dendrites and 579 gold-silver particles in 199 terminals.

The density of M2R immunogold particles (number of particles/analyzed surface) within plasmalemmal or cytoplasmic compartments was determined independently for dendrites showing cross-diameter  $>1\mu\text{m}$  or  $<1\mu\text{m}$  in both single-M2R and dual-VAChT+M2R dendrites. Batteries of Chi-square tests were applied to the data obtained to assess the statistical association among pairs regarding (1) M2R subcellular distribution, (2) dendritic size and (3) presence of concomitant VAChT-immunolabeling in those profiles. The cellular relationship between M2R- and VAChT-labeled profiles was assessed for all contacts/colocalizations between respectively immunoreactive profiles.

The electron micrographs used for the figures were acquired with an AMT digital camera (Advanced Microscopy Techniques Corporation, Danvers, MA) on a Microsmart Computer using a Windows 2000 operating system. To build and label the composite illustrations, Adobe Photoshop (version 7.0; Adobe Systems Inc., Mountain View, CA) software program was utilized for adjustment of brightness and sharpness of the digital images. The images were then imported into PowerPoint (Microsoft Office 2004 for Mac, Microsoft Corporation, Redmond, WA) to add the lettering and make the composite plate illustrations.

## RESULTS

Light microscopy showed M2R immunogold and immunoperoxidase labeling in somata and in many putative dendrites as well as in varicosities, which were most prevalent in the PPT and LTD, but also present in other portions of the MPT. In tissue processed for dual labeling, the somatic distribution of M2R immunoreactivity partially overlapped that of the VAChT even though there were also somata that were labeled exclusively for each of these proteins in both the PPT and LTD. Electron microscopy confirmed the primary localization of M2R and VAChT in some of the same as well as in separate somata and dendrites and also revealed the presence of M2R in axonal and glial profiles without VAChT labeling in each of these regions.

There were no significant variations between animals in the labeling area density (number of profiles per unit area) for M2R ( $F_{3,14}=0.744$ ;  $p=0.5435$ ), VAChT ( $F_{3,14}=0.603$ ;  $p=0.6238$ ) or VAChT+M2R ( $F_{3,14}=0.311$ ;  $p=0.8171$ ). The ANOVAs also showed that there were no statistically significant differences in labeling area density between PPT and LTD (M2R:  $F_{1,16}=0.685$ ;  $p=0.4200$ ; VAChT:  $F_{1,16}=0.069$ ;  $p=0.7968$ ; VAChT+M2R:  $F_{1,16}=0.317$ ;  $p=0.5810$ ). Since there were no significant inter-animal or inter-nuclei differences in the density of immunoreactivity and also no regional differences in the distribution of labeling in cellular profiles within the PPT and LTD, the data was pooled from different animals and both nuclei in the following descriptive analysis.

In tissue sections processed for reversed markers (M2R immunoperoxidase and VAChT immunogold), immunoperoxidase revealed a higher area density of M2R-labeled profiles than was seen using immunogold labeling in the MPT. However, the global distribution of labeling in different cellular compartments with either method was similar, and there were no apparent differences in frequencies or types of associations between differentially labeled profiles. Therefore, for the statistical analysis, we used only numbers obtained from the tissue in which M2R was detected with the immunogold

method that allows precise subcellular resolution of the receptor in relation to neurons whose processes were fully recognized by the diffuse immunoperoxidase labeling for the VAChT.

### **Localization of M2R labeling in somata with or without VAChT immunoreactivity**

The M2-containing somata comprised only slightly above 2% (42/1900) of the total M2-immunoreactive profiles within the MPT (Table 2). They displayed morphological heterogeneity and usually had a medium-large size, ranging from 11.6 to 33.2  $\mu\text{m}$  (shortest axis including the center of nucleus). In neuronal cell bodies, M2R immunoreactivity was distributed heterogeneously within the abundant cytoplasm. The M2R immunogold particles were frequently localized to endomembranes resembling smooth endoplasmic reticulum or to cisterns of the Golgi complex (Fig. 1). Thus, in these perikarya, the M2R-immunogold particles were frequently associated to Golgi lamellae or tubulovesicles (Fig. 1). Comparable proportions of M2R-immunogold particles were associated to cytoplasmic intramembranes in PPT ( $67.1\% \pm 2.9\%$ ) or LDT ( $71.4\% \pm 3.8\%$ ) somata, and no significant difference was observed between the two nuclei ( $F_{1,16}=0.131$ ;  $p=0.7338$ ). M2R-immunogold in somata was more rarely located on the intracellular face of the plasmalemma (Fig. 1A,B,C), which was usually not contacted by incoming afferent terminals.

Over 35% of the M2R-immunogold labeled somata ( $n=15$  out of 42) also contained VAChT-immunoperoxidase reaction product (Table 2). The VAChT labeling was intensely localized to intracytoplasmic tubulovesicles and, especially, the cisterns of the Golgi complex (Fig. 1C,D). The M2R subcellular distribution in dually-labeled somata was qualitatively similar to that seen in M2R single-labeled somata. The M2R-immunoreactive somata, either VAChT-labeled or not, had an extensive coverage by glial profiles (Fig. 1). Only one VAChT-immunoreactive soma did not contain M2R-immunogold in our sample; the rest ( $n=15$ , 93.8%) were dually-labeled (Table 3).



The M2R and M2R/VAChT-labeled somata were contacted mainly by unlabeled terminals (Fig. 1A) that were without recognizable synaptic specializations or formed more exclusively symmetric (76%) compared with asymmetric (24%) synapses. Although numerous VAChT-immunoreactive axon terminals were observed in the vicinity of M2R-immunolabeled somata, these terminals were rarely apposed or formed synapses with these somata. Seventeen percent ( $n=3$ ) of the terminals forming either symmetric or asymmetric synapses onto M2R-labeled somata contained VAChT immunoreactivity, and the remainder were without detectable immunoreactivity.

### **M2R targeting to dendrites defined by their content of VAChT and inputs from unlabeled, VAChT and/or M2R labeled terminals**

Most (1345/1900) M2R-labeled profiles in the MPT were dendrites (Table 2, Fig. 2). The majority of these dendrites were 0.4-2.8  $\mu\text{m}$  in diameter, but much larger M2R-labeled dendrites were also observed. M2 immunoreactivity was primarily localized to the plasma membrane in dendrites  $\leq 1 \mu\text{m}$  (Fig. 2A,B,C), while larger dendrites showed a more cytoplasmic M2R distribution (Fig. 2B, D) resembling that observed in somata. The dendritic plasmalemmal M2R-immunogold particles were located mainly on extrasynaptic portions of the plasma membrane away from inputs from axon terminals (Fig. 2A) and often apposed by glial profiles with (Fig. 2C) or without M2R immunoreactivity (Fig. 2B). These inputs included similar proportions of symmetric ( $n=305$ ) and asymmetric ( $n=307$ ) synapses mainly from axon terminals without detectable immunoreactivity ( $n=544$ ) (Table 3). However, the M2R-labeled dendrites were also recipient to terminals exclusively labeled for M2R ( $n=33$ ), VAChT ( $n=32$ ) or VAChT+M2R ( $n=3$ ) axon terminals (Fig. 2A,B,D; Table 3).

The preferential distribution of M2R-immunogold particles on plasma membrane of dendrites was quantitatively confirmed: thus, ANOVA proved a significantly higher M2R-immunogold density (mean number of gold particles per dendrite) related to the

plasma membrane ( $2.25 \pm 0.07$ ) in comparison with the cytoplasm ( $1.55 \pm 0.25$ ) in M2R-immunoreactive dendrites ( $F_{1,14}=7.230$ ;  $p<0.0176$ ). The predominant localization of M2R immunolabeling to the plasma membrane was, however, highly correlated to the dendritic size (ANOVA for interaction dendritic size x immunogold subcellular distribution:  $F_{1,12}=9.928$ ;  $p<0.0084$ ), being exclusive of PPT/LDT dendrites  $<1 \mu\text{m}$ ; in dendrites  $>1 \mu\text{m}$ , plasmalemmal and cytoplasmic localization of M2R-immunogold labeling were not significantly different (Fig. 3). Systematic counting of M2R-immunogold particles in dendrites showed that 69.5% of the total gold particles in small dendrites ( $<1 \mu\text{m}$ ) were in contact with the plasma membrane. A statistically significant association between dendritic size and subcellular location of M2R immunolabeling was also corroborated by using the Chi-square test for the raw number of M2R-immunogold particles (plasmalemmal vs. cytoplasmic) in M2R-labeled dendrites of different sizes ( $<1 \mu\text{m}$  vs.  $>1 \mu\text{m}$ ) ( $\chi^2_1=142.85$ ;  $p<0.0001$ ).

Approximately 16% of the M2R-immunogold labeled dendrites ( $n=212$  out of 1345) contained VAChT-immunoperoxidase reaction product (Table 2). The M2R subcellular distribution in dually-labeled dendrites was qualitatively similar to that seen in the general population of M2R-labeled dendrites, such that M2R-immunogold in the dual VAChT+M2R-labeled dendrites also had a prominent localization to the plasma membrane, although cytoplasmic distribution of M2R-immunogold was also observed (Figs. 3, 4). The preferential plasmalemmal M2R-labeling localization in dual VAChT+M2R-immunoreactive dendrites was not related their VAChT content. Thus, two-way ANOVAs (factors: subcellular distribution [plasmalemmal vs. cytoplasmic] x labeling type [single M2R vs. dual VAChT+M2R]) showed statistically significant variations in the mean M2R-immunogold density not related to the type of labeling (distribution:  $F_{1,28}=6.627$ ;  $P=0.0156$ ; distribution x labeling:  $F_{1,28}=0.496$ ;  $P=0.4871$ ) (Fig. 3). Furthermore, no statistical differences were observed in the M2R-immunogold density between single- and dual-labeled dendrites (ANOVA factor, labeling type:

$F_{1,28}=0.830$ ;  $P=0.3702$ ). Moreover, independent ANOVA for M2R-immunogold localization in the VAchT+M2R-labeled dendrites indicated that, similar to the entire group of M2R-immunolabeled dendrites, the dual-labeled VAchT+M2R dendrites had significantly higher plasmalemmal versus cytoplasmic densities of M2R-immunogold in the small dendrites ( $F_{1,6}=8.746$ ;  $P=0.0254$ ), but not in large dendrites ( $F_{1,6}=0.452$ ;  $P=0.5264$ ). Chi-square test for the number of M2R-immunogold particles in those dually VAchT+M2R dendrites also revealed that statistically significant association among M2R subcellular distribution (cytoplasmic vs. plasmalemmal) and the dendritic size (small vs. large) ( $\chi^2_1=23.518$ ;  $p<0.0001$ ), and as said above this occurred regardless of the presence or absence of VAchT immunolabeling in the dendrites (Table 2).

Finally, Chi-square test for M2R-immunogold density showed an absence of statistically significant association between the type of labeling (dual vs. single) and the dendritic size (diameter  $<1\mu\text{m}$  vs diameter  $>1\mu\text{m}$ ) ( $\chi^2_1=0.045$ ;  $p=0.8327$ ), such that the higher M2R-immunolabeling density in large dendrites was significant both in single and dual dendrites ( $F_{1,28}=10.289$ ;  $P=0.0033$ ). The proportion of dual dendrites was, however, much greater within the large ( $n=86/407$ , 21.1%) than within the small ( $n=126/938$ , 13.4%) profiles, indicating that, although M2R-labeling density was similar, and not related to dendritic size, dual labeled profiles are more frequently sampled among the large dendrites, as shown by a significant association between type of labeling and dendritic size when assessing the number of M2R-immunolabeled profiles ( $\chi^2_1=12.666$ ;  $p=0.0004$ ). Dendrites containing both M2R and VAchT received symmetric and asymmetric inputs mainly from unlabeled terminals (Fig. 4A,B) ( $n=50$ ), but also from some M2R- ( $n=8$ ) or VAchT-labeled ( $n=3$ ) axon terminals (Figs. 4C,D).

The dual dendrites represented about 43% of the total VAchT-immunolabeled dendrites ( $n=488$ ). The remainder were VAchT-labeled dendrites in which M2R could not be detected ( $n=276$ ; Table 2).

### **Distribution of M2R labeling in axons targeting VAChT- and/or M2R-labeled dendrites**

Approximately 11 percent (n=199) of M2R-immunoreactive profiles were identified as axon terminals (Table 2) based on their size and content of synaptic vesicles. M2R-immunoreactive axon terminals ranged from 0.3 to 1.6  $\mu\text{m}$  in diameter, and contained all small synaptic vesicles (SSVs) (40-60 nm in diameter) or many SSVs combined with one or more large dense core vesicles. There was, however, no apparent correlation between the density of M2R-immunoreactivity and either the size or vesicle content of axon terminals.

M2R-immunogold was chiefly localized to discrete segments of the presynaptic and non-synaptic plasma membranes of axon terminals (Figs. 2C, 5D). Less frequently, M2R-immunogold particles in axon terminals had an intracytoplasmic localization, and some of the smaller particles overlay SSVs in these terminals (Fig. 2C, D). The M2R-immunogold density (mean number of gold particles per terminal) associated to the plasma membrane ( $2.25 \pm 0.07$ ) was significantly higher than that related to the cytoplasm ( $1.55 \pm 0.25$ ) in M2R-immunoreactive terminals (ANOVA:  $F_{1,14}=7.230$ ;  $p < 0.0176$ ).

The M2R-immunolabeled axon terminals established many associations with adjacent neuropil profiles that included axodendritic synapses (Fig. 2) as well as appositional contacts with axon terminals and/or glial processes (Figs. 5, 6). As observed in single thin sections, 36.7% (73/199) of the M2-labeled terminals formed recognizable synaptic specializations in the plane of section. Their postsynaptic targets were mainly unlabeled dendrites (n=36), but also included dendrites containing solely M2 (n=28), solely VAChT (n=1) or both markers (n=8). Regarding the morphology of the synapses, the M2-labeled terminals formed quite balanced symmetric (n=41) and asymmetric (n=32) contacts (Table 3).

In contrast with somata and dendrites, M2R-labeled axon terminals seldom contained VAChT-immunoreactivity. Of the observed M2R-immunogold labeled terminals, 94.5% (n=188; Table 2) were devoid of the VAChT immunoperoxidase reaction product seen in the remaining other terminals (Fig. 6). These dually VAChT+M2R-labeled axon terminals comprised only 5.5% (11/199) of the M2R- and (2.5%; 11/435) of the VAChT-labeled terminals (Table 2). The subcellular distribution of M2R-immunogold and synaptic associations of the dual labeled terminals (Fig. 6) were similar to that described above for axon terminals containing M2R, but not VAChT immunoreactivity (Table 3).

### **VAChT-labeled terminals targeting M2R dendrites or apposing M2R terminals**

VAChT-immunolabeled axon terminals were abundant throughout the MPT (n=435, Table 2). The VAChT-immunoreactive axon terminals frequently apposed (Fig. 6A), and in some cases formed recognizable symmetric (n=18) or asymmetric (n=17) synapses with M2R-labeled dendrites (Table 3). Separate VAChT- and M2R-immunoreactive terminals also converged onto common dendritic targets, some of which also were labeled for the M2R (Fig. 5B). More rarely, M2R-immunogold particles were located along segment of the axonal plasma membrane contacted by VAChT-immunoreactive terminals (Fig. 5D). In these cases, some M2R-immunogold particles were usually localized on the segment of plasma membrane apposed to the VAChT-immunoreactive terminal.

### **Axonal and glial M2R labeling**

Small unmyelinated axons immunoreactive for M2R comprised nearly 13.5% (254/1900) of the total M2-labeled profiles in PPT/LDT and almost never contained VAChT (Table 2). M2R-immunogold labeling in small unmyelinated axons was detected

either on the plasma membrane or in the cytoplasm. Less than 1% of the total M2-immunoreactive profiles (14/1900) were myelinated axons (Table 2).

M2R-immunolabeling was readily detected in select glial profiles throughout the MPT (n=46; 2.4% of total M2R-labeled profiles). M2R-immunogold particles were primarily localized to the plasma membrane of glial processes (Figs. 2C, 5C) that were apposed to M2R-immunolabeled dendrites (Fig. 2C) or to VAChT-immunoreactive axonal profiles (Fig. 5C). These glial processes often contained glial filaments and formed gap junctions that are characteristic of astrocytes (Fig. 5C).

## DISCUSSION

We have shown that in both the PPT and LDT, M2R immunoreactivity is mainly localized to extrasynaptic plasma membranes and endomembranes within the cytoplasm of somatodendritic profiles, some of which contain VAChT (Fig. 7). This suggests, respectively, potential sites for M2R modulation of postsynaptic excitability, as well as synthesis and recycling in PPT/LDT cholinergic and non-cholinergic neurons. In addition, we show M2R located on the plasma membrane in axon terminals that are largely devoid of VAChT immunoreactivity. This distribution and the more rarely seen M2R labeling in small axonal and glial processes without VAChT labeling are consistent with M2R involvement in modulation of the presynaptic release of transmitters other than Ach and in glial signaling in the PPT/LTD complex. Together, these results suggest multiple sites for M2R-activation that could significantly affect the output of cholinergic and non-cholinergic neurons in the MPT (Fig. 7). Since no regional differences have been detected between PPT and LDT regarding M2R localization or association with VAChT, the following discussion predictably includes both nuclei. Any individual specific repercussions for either of them are mentioned if pertinent.

### Expression of M2R in PPT/LDT somata and dendrites

The localization of M2R to plasma membranes in MPT somata and dendrites with or without VAChT is consistent with electrophysiological evidence indicating that M2R activation contributes to G protein-coupled inwardly rectifying potassium (GIRK) channel-mediated membrane hyperpolarization and inhibition of R-channel-mediated spike-evoked  $\text{Ca}^{2+}$  transients produced in MPT neurons by muscarinic agonists (Kohlmeier et al., 2012). The prominent somatodendritic distribution of M2Rs in the many brain areas studied so far of both GIRK channels (Ponce et al., 1996) and R-type calcium channels (Parajuli et al., 2012) further supports M2R-mediated signal transduction on plasma membranes of MPT neurons. Our demonstration of a

predominant plasmalemmal distribution of M2R in dendritic profiles, only some of which contained VAChT-immunoreactivity suggests that M2R is involved in ionic interchange and second messenger function in both cholinergic and non-cholinergic neurons of PPT/LDT. The more commonly observed intracytoplasmic versus plasmalemmal M2R labeling in somata is consistent with previous reports of scarce axosomatic cholinergic synapses onto PPT/LDT neurons (Steininger et al., 1997; Garzón and Pickel, 2000). Extrasynaptic plasma membranes of dendrites are likely to be the primary sites for M2R activation, as has been suggested for other G-protein-coupled receptors (Hille, 1992) and specifically indicated by the surface distribution of M2Rs in dendrites within other brain regions (Bernard et al., 1998; Garzón and Pickel, 2006, 2013; Csaba et al., 2013; Muller et al., 2013). The preferential distribution of M2R-immunogold particles on extrasynaptic plasma membranes of dendrites is consistent with M2R activation by extrasynaptic diffusion of Ach from release sites (Umbriaco et al., 1994; Garzón and Pickel, 2006). Moreover, the large incidence of M2R-labeled dendrites without recognizable synapses or contacts from VAChT-immunoreactive profiles envisages cholinergic volume transmission as an accountable intercellular signaling mode in the PPT/LDT.

The present observation of M2R-labeling along cisterns of the Golgi apparatus, SER, and tubulovesicles suggests the involvement of these organelles in the synthesis, assembly, transport, recycling and/or degradation of membranes containing M2R in PPT/LDT neurons, which is similar to that observed previously in ventral tegmental area (Garzón and Pickel, 2006). M2R localization in endomembranes involved in the dynamic trafficking of proteins along microtubules is further suggested by the similarity of these membranes to early endosomes participating in G protein-coupled receptor transport and recycling (Bernard et al., 1998; Delaney et al., 2002; Seachrist and Ferguson, 2003). M2R undergoes agonist-induced internalization in striatal interneurons *in vivo*, such that M2R targeting to the somatodendritic plasma membrane



and its availability at the neuronal cell surface is finely regulated by the cholinergic microenvironment (Bernard et al., 1998; Bloch et al., 2003). These findings together suggest that a fraction of M2R belongs to a receptor pool inaccessible to extracellular Ach, which may undergo activity-dependent mobilization to the plasma membrane, as shown previously in a model of chronic hypercholinergy (Bernard et al., 2003).

### **Potential sites for M2R activation in PPT/LDT dendrites**

We observed substantial M2R immunogold labeling associated with the plasma membrane and cytoplasmic organelles in large as well as in small and presumably more distal dendrites. The dendritic localization of M2R in many neurons that do not express VAChT is consistent with previous studies indicating that this receptor is not only an autoreceptor in cholinergic terminals, but also mediates both pre- and post-synaptic actions of Ach in non-cholinergic PPT/LDT neurons (Levey et al., 1991; Garzón and Pickel, 2006; Kohlmeier et al., 2012). Some GABA neurons in the MPT are known to contain M2R (Brischoux et al., 2008). Glutamatergic neurons existing in the PPT/LDT (Wang and Morales, 2009) could also belong to the non-cholinergic PPT/LDT neurons expressing M2R. The role of M2R heteroreceptors has also been reported in other brain areas such as the hippocampus (Rouse et al., 2000) and the ventral tegmental area (Garzón and Pickel, 2006).

The localization of M2Rs near axon terminals that formed equally prevalent asymmetric or symmetric synapses onto M2R-immunoreactive dendrites suggests that both excitatory and inhibitory neurotransmitters may modify postsynaptic responses to Ach in PPT/LDT. Likewise, Ach may play a role in postsynaptic modulation of the excitation or inhibition produced by glutamate and other neurotransmitters present in extrinsic and intrinsic local neurons within PPT/LDT (Lai et al., 1993; Wang and Morales, 2009; Kohlmeier et al., 2012)

**M2R activation in cholinergic PPT/LDT neurons**

M2R localization on plasma membranes of many VAChT-immunolabeled dendrites provides a cellular substrate conducive to inhibitory autoreceptor function of M2Rs in PPT/LDT cholinergic neurons (Luebke et al., 1993; Leonard and Llinás, 1984; Ye et al., 2010; Kohlmeier et al., 2012). Likewise, M2R observation in PPT/LDT cholinergic somata and dendrites further strengthens purported M2R function as an inhibitory autoreceptor at cholinergic terminals derived from PPT/LDT within target regions. Thus, presynaptic M2R autoreceptors may mediate Ach-induced release in axon terminals originating from MPT cholinergic neurons in the pontine reticular formation (Roth et al., 1996; Baghdoyan et al., 1998) and ventral tegmental area (Forster and Blaha, 2000; Garzón and Pickel, 2006). These could have significant effects, respectively, in sleep-wake regulation (Gnadt and Pegram, 1986; Reinoso-Suárez et al., 1994; Garzón et al., 1997, 1998) and rewarding behaviors (Westerink et al., 1996, 1998; Enrico et al., 1998). Thus, our results have important implications for understanding the multiple M2R-mediated actions of Ach in the behaviors that are dependent on output of cholinergic and non-cholinergic neurons in the MPT.

**Presynaptic M2R in relation to cholinergic and non-cholinergic neurons**

Our detection of M2R immunoreactivity on the plasma membrane of axon terminals providing synaptic input to PPT/LDT dendrites suggests that M2Rs mediate the presynaptic regulation of neurotransmitter release onto MPT neurons (Gilsbach and Hein, 2008). These results are consistent with the known M2R involvement in autoreceptor and heteroreceptor modulation of presynaptic neurotransmitter release in other brain regions (Baghdoyan et al., 1998; Rousse et al., 2000; Parnas et al., 2005).

The additional observation of M2R immunolabeling on some vesicular membranes in axon terminals may also support a M2R-mediated inhibition of calcium-dependent neurotransmitter release through interference in coupling processes

between receptor activation and neurotransmitter secretion (Brown and Sihra, 2008). Activation of muscarinic receptors may modulate neurotransmitter release through vesicular docking adjustment (Bourne, 1988; Mizoguchi et al., 1990). This should be conceivable in cholinergic axons, where Ach is available to activate vesicular M2R. However, since VAChT was rarely detected together with M2R in axon terminals the M2R-mediated presynaptic actions are more likely to serve as plasmalemmal heteroreceptor rather than an autoreceptor in the MPT. The M2R vesicular localization may reflect, instead, receptor recycling sites and/or vesicles mediation in transportation to and from functional sites both in cholinergic and non-cholinergic terminals (Mukherjee et al., 1997; Sudhof, 2004). The coexpression of M2R and VAChT in dendrites, but rarely in axon terminals, suggests important differences in the dendritic and axonal targeting of M2Rs.

M2R labeling was identified in axon terminals that made asymmetric or symmetric synapses. M2R observation in axon terminals forming asymmetric excitatory-type synapses supports previous studies suggesting the presence of M2Rs in PPT/LDT glutamatergic terminals based on the effectiveness of M2R antagonists in blocking the carbachol-induced decreases in miniature excitatory postsynaptic currents recorded in rat PPT *in vitro* (Ye et al., 2010). Presynaptic M2R in glutamatergic terminals is well documented in spinal primary afferents (Zhang et al., 2007) and in excitatory glutamatergic inputs to hypoglossal motoneurons (Bellingham and Berger, 1996), bed nucleus of the stria terminalis (Guo et al., 2012) and hippocampus (Zheng et al., 2001). The observation of M2R in axon terminals forming symmetric inhibitory-type synapses advocates for M2R involvement in modulation of GABA release in PPT/LDT. This conclusion is supported by numerous earlier studies that implicate presynaptic M2Rs in the inhibition of GABA release in the cerebral cortex and other brain regions (Fukudome et al., 2004; Salgado et al., 2007).

We observed a paucity of dual M2R/VAChT-labeled axon terminals in PPT/LDT although many nearby terminals in this area contained exclusively M2R or VAChT immunoreactivity. This suggests that the presynaptic M2R acts more like a heteroreceptor than autoreceptor in the PPT/LDT complex, which is in marked contrast to the well-known involvement of M2Rs in the presynaptic modulation of cholinergic axons described in other brain regions (see above). This raises the possibility of a differential M2R distribution in somatodendritic versus axonal domains in cholinergic PPT/LDT neurons. In addition, however, some M2R-labeled axons and axon terminals directly apposed VAChT-immunoreactive terminals. This finding suggests that Ach may affect the release of other neurotransmitters that can in turn regulate Ach release.

We observed M2R labeling in some of the terminals providing input to M2R-containing dendrites. These terminals were morphologically heterogeneous and might have comprised those containing either glutamate or GABA (see above). Hence, M2R-elicited changes in the release of these neurotransmitters may be a meaningful synaptic mechanism to control the output of a particular subpopulation of PPT/LDT neurons that also expresses M2Rs.

### **M2R glial labeling in PPT/LDT**

The glial M2R distribution in PPT/LDT is in agreement with previous ultrastructural findings in the ventral tegmental area (Garzón and Pickel, 2006). The findings are consistent with former evidence gathered *in vitro* showing the presence of muscarinic receptors in glial cells, as well as glial responses to M2R agonists (Porter and McCarthy, 1997; Elhusseiny et al., 1999; Roda et al., 2008). In our study, astrocytic processes were frequently seen apposed to segments of the M2R-containing dendritic plasmalemma. The glia may potentially facilitate Ach diffusion within the neuropil to reach receptive sites on extrasynaptic domains of the postsynaptic neuron. Moreover, the observed prevalence of M2R-immunolabeled astrocytic profiles apposing or

enfolding M2R- and/or VAChT-containing profiles in our samples further suggests that M2R-mediated astrocytic responses could notably affect the synaptic microenvironment in PPT/LDT. The M2R distribution in glial processes in the PPT/LDT may also provide a cellular substrate for cholinergic regulation of astrocytic calcium signaling involved in stimulus-specific synaptic plasticity in pontine tegmental nuclei, which is comparable to that previously shown by *in vitro* studies the cerebral cortex (Takata et al., 2011; Chen et al., 2012).

### CONFLICT OF INTERESTS

The authors declare that they have no conflict of interest.

### ROLE OF AUTHORS

The two authors had full access to all the data in the study and take responsibility for the integrity of the data and the accuracy of the data analysis. They equally contributed to the design and implementation of the experiments as well as manuscript preparation. The first author (MG) is largely responsible for collection of images and data analysis.

**LITERATURE CITED**

- Arvidsson U, Riedl M, Elde R, Meister B. 1997. Vesicular acetylcholine transporter (VAChT) protein: a novel and unique marker for cholinergic neurons in the central and peripheral nervous systems. *J Comp Neurol* 378: 454-467.
- Baghdoyan HA. 1997. Location and quantification of muscarinic receptor subtypes in rat pons: implications for REM sleep generation. *Am J Physiol* 273: R896-R904.
- Baghdoyan HA, Lydic R, Callaway CW, Hobson JA. 1989. The carbachol-induced enhancement of desynchronized sleep signs is dose dependent and antagonized by centrally administered atropine. *Neuropsychopharmacology* 2:67-79.
- Baghdoyan HA, Lydic R, Fleegal MA. 1998. M2 muscarinic autoreceptors modulate acetylcholine release in the medial pontine reticular formation. *J Pharmacol Exp Ther* 286:1446-1452.
- Baghdoyan HA, Mallios VJ, Duckrow RB, Mash DC. 1994. Localization of muscarinic receptor subtypes in brain stem areas regulating sleep. *Neuroreport* 5:1631-1634.
- Bejanin S, Cervini R, Mallet J, Berrard S. 1994. A unique gene organization for two cholinergic markers, choline acetyltransferase and a putative vesicular transporter of acetylcholine. *J Biol Chem* 269:21944-21947.
- Bellingham MC, Berger AJ. 1996. Presynaptic depression of excitatory synaptic inputs to rat hypoglossal motoneurons by muscarinic M2 receptors. *J Neurophysiol* 76:3758-3770.
- Bernard V, Brana C, Liste I, Lockridge O, Bloch B. 2003. Dramatic depletion of cell surface m2 muscarinic receptor due to limited delivery from intracytoplasmic stores in neurons of acetylcholinesterase-deficient mice. *Mol Cell Neurosci* 23:121-133.
- Bernard V, Laribi O, Levey AI, Bloch B. 1998. Subcellular redistribution of m2 muscarinic acetylcholine receptors in striatal interneurons in vivo after acute cholinergic stimulation. *J Neurosci* 18:10207-10218.
- Billard W, Binch H 3rd, Crosby G, McQuade RD. 1995. Identification of the primary muscarinic autoreceptor subtype in rat striatum as m2 through a correlation of in vivo microdialysis and in vitro receptor binding data. *J Pharmacol Exp Ther* 273:273-279.

- Blaha CD, Allen LF, Das S, Inglis WL, Latimer MP, Vincent SR, Winn P. 1996. Modulation of dopamine efflux in the nucleus accumbens after cholinergic stimulation of the ventral tegmental area in intact, pedunculo pontine tegmental nucleus-lesioned, and laterodorsal tegmental nucleus-lesioned rats. *J Neurosci* 16:714-722.
- Blaha CD, Winn P. 1993. Modulation of dopamine efflux in the striatum following cholinergic stimulation of the substantia nigra in intact and pedunculo pontine tegmental nucleus-lesioned rats. *J Neurosci* 13:1035-1044.
- Bloch B, Bernard V, Dumartin B. 2003. "In vivo" intraneuronal trafficking of G protein coupled receptors in the striatum: regulation by dopaminergic and cholinergic environment. *Biol Cell* 95:477-488.
- Bonner TI, Buckley NJ, Young AC, Brann MR. 1987. Identification of a family of muscarinic acetylcholine receptor genes. *Science* 237:527-532.
- Bonner TI, Young AC, Brann MR, Buckley NJ. 1988. Cloning and expression of the human and rat m5 muscarinic acetylcholine receptor genes. *Neuron* 1:403-410.
- Boucetta S, Cissé Y, Mainville L, Morales M, Jones BE. 2014. Discharge profiles across the sleep-waking cycle of identified cholinergic, GABAergic, and glutamatergic neurons in the pontomesencephalic tegmentum of the rat. *J Neurosci* 34:4708-4727. doi: 10.1523/JNEUROSCI.2617-13.2014.
- Boucetta S, Jones BE. 2009. Activity profiles of cholinergic and intermingled GABAergic and putative glutamatergic neurons in the pontomesencephalic tegmentum of urethane-anesthetized rats. *J Neurosci* 29:4664-4674. doi: 10.1523/JNEUROSCI.5502-08.2009.
- Bourne HR. 1988. Do GTPases direct membrane traffic in secretion? *Cell* 53:669-671.
- Brischoux F, Mainville L, Jones BE. 2008. Muscarinic-2 and orexin-2 receptors on GABAergic and other neurons in the rat mesopontine tegmentum and their potential role in sleep-wake state control. *J Comp Neurol* 510:607-630. doi: 10.1002/cne.21803.
- Brown DA, Sihra TS. 2008. Presynaptic signaling by heterotrimeric G-proteins. *Handb Exp Pharmacol* 184:207-60.
- Buckley NJ, Bonner TI, Brann MR. 1988. Localization of a family of muscarinic receptor

- mRNAs in rat brain. *J Neurosci* 8:4646-4652.
- Butcher LL, Oh JD, Woolf NJ, Edwards RH, Roghani A. 1992. Organization of central cholinergic neurons revealed by combined in situ hybridization histochemistry and choline-O-acetyltransferase immunocytochemistry. *Neurochem Int* 21:429-445.
- Calabresi P, Centonze D, Pisani A, Sancesario G, North RA, Bernardi G. 1998. Muscarinic IPSPs in rat striatal cholinergic interneurons. *J Physiol* 510:421-427.
- Chan J, Aoki C, Pickel VM. 1990. Optimization of differential immunogold-silver and peroxidase labeling with maintenance of ultrastructure in brain sections before plastic embedding. *J Neurosci Methods* 33:113-127.
- Chapman CA, Yeomans JS, Blaha CD, Blackburn JR. 1997. Increased striatal dopamine efflux follows scopolamine administered systemically or to the tegmental pedunculo-pontine nucleus. *Neuroscience* 76:177-186.
- Chen J, Nakamura M, Kawamura T, Takahashi T, Nakahara D. 2006. Roles of pedunculo-pontine tegmental cholinergic receptors in brain stimulation reward in the rat. *Psychopharmacology (Berl)* 184:514-522.
- Chen N, Sugihara H, Sharma J, Perea G, Petravic J, Le C, Sur M. 2012. Nucleus basalis-enabled stimulus-specific plasticity in the visual cortex is mediated by astrocytes. *Proc Natl Acad Sci USA* 109:E2832-E2841. doi: 10.1073/pnas.1206557109.
- Cid-Pellitero E, Garzón M. 2011. Hypocretin1/OrexinA axon targeting of laterodorsal tegmental nucleus neurons projecting to the rat medial prefrontal cortex. *Cereb Cortex* 21:2762-2773. doi: 10.1093/cercor/bhr070.
- Cornwall J, Cooper JD, Phillipson OT. 1990. Afferent and efferent connections of the laterodorsal tegmental nucleus in the rat. *Brain Res Bull* 25:271-284.
- Csaba Z, Krejci E, Bernard V. 2013. Postsynaptic muscarinic m2 receptors at cholinergic and glutamatergic synapses of mouse brainstem motoneurons. *J Comp Neurol* 521:2008-2024. doi: 10.1002/cne.23268.
- Delaney KA, Murph MM, Brown LM, Radhakrishna H. 2002. Transfer of M2 muscarinic acetylcholine receptors to clathrin-derived early endosomes following clathrin-independent endocytosis. *J Biol Chem* 277:33439-33446.



- Di Giovanni G, Shi WX. 2009. Effects of scopolamine on dopamine neurons in the substantia nigra: role of the pedunculo pontine tegmental nucleus. *Synapse* 63:673-80. doi: 10.1002/syn.20650.
- Elhusseiny A, Cohen Z, Olivier A, Stanimirović DB, Hamel E. 1999. Functional acetylcholine muscarinic receptor subtypes in human brain microcirculation: identification and cellular localization. *J Cereb Blood Flow Metab* 19:794-802.
- Enrico P, Bouma M, De Vries JB, Westerink BHC. 1998. The role of afferents to the ventral tegmental area in the handling stress-induced increase in the release of dopamine in the medial prefrontal cortex: a dual-probe microdialysis in the rat brain. *Brain Res* 779:205-213.
- Erickson JD, Varoqui H, Schäfer MK, Modi W, Diebler M-F, Weihe E, Rand J, Eiden LE, Bonner TI, Usdin TB. 1994. Functional identification of a vesicular acetylcholine transporter and its expression from a "cholinergic" gene locus. *J Biol Chem* 269:21929-21932.
- Forster GL, Blaha CD. 2000. Laterodorsal tegmental stimulation elicits dopamine efflux in the rat nucleus accumbens by activation of acetylcholine and glutamate receptors in the ventral tegmental area. *Eur J Neurosci* 12:3596-3604.
- Frey KA, Howland MM. 1992. Quantitative autoradiography of muscarinic cholinergic receptor binding in the rat brain: distinction of receptor subtypes in antagonist competition assays. *J Pharmacol Exp Ther* 263:1391-1400.
- Fukudome Y, Ohno-Shosaku T, Matsui M, Omori Y, Fukaya M, Tsubokawa H, Taketo MM, Watanabe M, Manabe T, Kano M. 2004. Two distinct classes of muscarinic action on hippocampal inhibitory synapses: M2-mediated direct suppression and M1/M3-mediated indirect suppression through endocannabinoid signalling. *Eur J Neurosci* 19:2682-2692.
- Garzón M, de Andrés I, Reinoso-Suárez F. 1997. Neocortical and hippocampal electrical activities are similar in spontaneous and cholinergic-induced REM sleep. *Brain Res* 766:266-270.
- Garzón M, de Andrés I, Reinoso-Suárez F. 1998. Sleep patterns after carbachol delivery in the ventral oral pontine tegmentum of the cat. *Neuroscience* 83:1137-1144.

- Garzón M, Pickel VM. 2000. Dendritic and axonal targeting of the vesicular acetylcholine transporter to membranous cytoplasmic organelles in laterodorsal and pedunculo pontine tegmental nuclei. *J Comp Neurol* 419:32-48.
- Garzón M, Pickel VM. 2006. Subcellular distribution of M2 muscarinic receptors in relation to dopaminergic neurons of the rat ventral tegmental area. *J Comp Neurol* 498:821-839.
- Garzón M, Pickel VM. 2013. Somatodendritic targeting of M5 muscarinic receptor in the rat ventral tegmental area: implications for mesolimbic dopamine transmission. *J Comp Neurol* 521:2927-2946. doi: 10.1002/cne.23323.
- Garzón M, Vaughan RA, Uhl GR, Kuhar MJ, Pickel VM. 1999. Cholinergic axon terminals in the ventral tegmental area target a subpopulation of neurons expressing low levels of the dopamine transporter. *J Comp Neurol* 410:197-210.
- Giltsbach R, Hein L. 2008. Presynaptic metabotropic receptors for acetylcholine and adrenaline/noradrenaline. *Handb Exp Pharmacol* 184:261-88.
- Gnadt JW, Pegram GV. 1986. Cholinergic brainstem mechanisms of REM sleep in the rat. *Brain Res* 384:29-41.
- Gray EG. 1959. Axosomatic and axo-dendritic synapses of the cerebral cortex: an electron microscopic study. *J Anat* 93:420-433.
- Guo JD, Hazra R, Dabrowska J, Muly EC, Wess J, Rainnie DG. 2012. Presynaptic muscarinic M(2) receptors modulate glutamatergic transmission in the bed nucleus of the stria terminalis. *Neuropharmacology* 62:1671-1683. doi: 10.1016/j.neuropharm.2011.11.013.
- Hille B. 1992. G protein-coupled mechanisms and nervous signaling. *Neuron* 9:187-195.
- Horner RL, Kubin L. 1999. Pontine carbachol elicits multiple rapid eye movement sleep-like neural events in urethane-anaesthetized rats. *Neuroscience* 93:215-226.
- Hsu SM, Raine L, Fanger H. 1981. The use of avidin-biotin-peroxidase complex (ABC) in immunoperoxidase technique: a comparison between ABC and unlabeled antibody (peroxidase) procedures. *J Histochem Cytochem* 29:577-599.
- Jones BE. 1993. The organization of central cholinergic systems and their functional importance in sleep-waking states. *Prog Brain Res* 98:61-71.

- Kodama T, Takahashi Y, Honda Y. 1990. Enhancement of acetylcholine release during paradoxical sleep in the dorsal tegmental field of the cat brain stem. *Neurosci Lett* 114:277-282.
- Kohlmeier KA, Ishibashi M, Wess J, Bickford ME, Leonard CS. 2012. Knockouts reveal overlapping functions of M(2) and M(4) muscarinic receptors and evidence for a local glutamatergic circuit within the laterodorsal tegmental nucleus. *J Neurophysiol* 108:2751-2766. doi: 10.1152/jn.01120.2011.
- Kubo T, Fukuda K, Mikami A, Maeda A, Takahashi H, Mishina M, Haga T, Haga K, Ichiyama A, Kangawa K, Kojima M, Matsuo H, Hirose T, Numa S. 1986. Cloning, sequencing and expression of complementary DNA encoding the muscarinic acetylcholine receptor. *Nature* 323:411-416.
- Lai YY, Clements JR, Siegel JM. 1993. Glutamatergic and cholinergic projections to the pontine inhibitory area identified with horseradish peroxidase retrograde transport and immunohistochemistry. *J Comp Neurol* 336(3):321-330.
- Leonard CS, Llinás R. 1994. Serotonergic and cholinergic inhibition of mesopontine cholinergic neurons controlling REM sleep: an in vitro electrophysiological study. *Neuroscience* 59:309-330.
- Leranth C, Pickel VM. 1989. Electron microscopic pre-embedding double immunostaining methods. In: *Tract tracing methods 2, recent progress*, L. Heimer and L. Zaborsky, eds., pp. 129-172, Plenum, New York.
- Levey AI, Kitt CA, Simonds WF, Price DL, Brann MR. 1991. Identification and localization of muscarinic acetylcholine receptor proteins in brain with subtype-specific antibodies. *J Neurosci* 11:3218-3226.
- Lodge DJ, Grace AA. 2006. The laterodorsal tegmentum is essential for burst firing of ventral tegmental area dopamine neurons. *Proc Natl Acad Sci USA* 103:5167-5172.
- Luebke JI, McCarley RW, Greene RW. 1993. Inhibitory action of muscarinic agonists on neurons in the rat laterodorsal tegmental nucleus in vitro. *J Neurophysiol* 70:2128-2135.
- Lydic R, Baghdoyan HA. 1993. Pedunculopontine stimulation alters respiration and increases ACh release in the pontine reticular formation. *Am J Physiol* 264:R544-R54.

- Lydic R, Baghdoyan HA, Lorinc Z. 1991. Microdialysis of cat pons reveals enhanced acetylcholine release during state-dependent respiratory depression. *Am J Physiol* 261:R766-R770.
- Maloney KJ, Mainville L, Jones BE. 1999. Differential c-Fos expression in cholinergic, monoaminergic, and GABAergic cell groups of the pontomesencephalic tegmentum after paradoxical sleep deprivation and recovery. *J Neurosci* 19:3057-3072.
- Miller AD, Blaha CD. 2004. Nigrostriatal dopamine release modulated by mesopontine muscarinic receptors. *Neuroreport* 15:1805-1808.
- Mizoguchi A, Kim S, Ueda T, Kikuchi A, Yorifuji H, Hirokawa N, Takai Y. 1990. Localization and subcellular distribution of smg p25A, a ras p21-like GTP-binding protein, in rat brain. *J Biol Chem* 265:11872-11879.
- Moreno-Balandrán E, Garzón M, Bódalo C, Reinoso-Suárez F, de Andrés I. 2008. Sleep-wakefulness effects after microinjections of hypocretin 1 (orexin A) in cholinceptive areas of the cat oral pontine tegmentum. *Eur J Neurosci* 28:331-341. doi: 10.1111/j.1460-9568.2008.06334.x.
- Mukherjee S, Ghosh RN, Maxfield FR. 1997. Endocytosis. *Physiol Rev* 77:759-803.
- Muller JF, Mascagni F, Zaric V, McDonald AJ. 2013. Muscarinic cholinergic receptor M1 in the rat basolateral amygdala: ultrastructural localization and synaptic relationships to cholinergic axons. *J Comp Neurol* 521:1743-1759. doi: 10.1002/cne.23254.
- Parajuli LK, Nakajima C, Kulik A, Matsui K, Schneider T, Shigemoto R, Fukazawa Y. 2012. Quantitative regional and ultrastructural localization of the Ca(v)2.3 subunit of R-type calcium channel in mouse brain. *J Neurosci* 32:13555-13567.
- Parnas H, Slutsky I, Rashkovan G, Silman I, Wess J, Parnas I. 2005. Depolarization initiates phasic acetylcholine release by relief of a tonic block imposed by presynaptic M2 muscarinic receptors. *J Neurophysiol* 93:3257-3269.
- Peralta EG, Winslow JW, Peterson GL, Smith DH, Ashkenazi A, Ramachandran J, Schimerlik MI, Capon DJ. 1987. Primary structure and biochemical properties of an M2 muscarinic receptor. *Science* 236:600-605.
- Peters A, Palay SL, Webster HD. 1991. The fine structure of the nervous system: neurons and their supporting cells. New York: Oxford University Press.

- Pickel VM, Douglas J, Chan J, Gamp PD, Bunnett NW. 2000. Neurokinin 1 receptor distribution in cholinergic neurons and targets of substance P terminals in the rat nucleus accumbens. *J Comp Neurol* 423:500-511.
- Ponce A, Bueno E, Kentros C, Vega-Saenz de Miera E, Chow A, Hillman D, Chen S, Zhu L, Wu MB, Wu X, Rudy B, Thornhill WB. 1996. G-protein-gated inward rectifier K<sup>+</sup> channel proteins (GIRK1) are present in the soma and dendrites as well as in nerve terminals of specific neurons in the brain. *J Neurosci* 16:1990-2001.
- Porter JT, McCarthy KD. 1997. Astrocytic neurotransmitter receptors in situ and in vivo. *Prog Neurobiol* 51:439-55.
- Reinoso-Suárez F, de Andrés I, Rodrigo-Angulo ML, Garzón M. 2001. Brain structures and mechanisms involved in the generation of REM sleep. *Sleep Med Rev* 5:63-77.
- Reinoso-Suárez F, De Andrés I, Rodrigo-Angulo ML, Rodríguez-Veiga E. 1994. Location and anatomical connections of a paradoxical sleep induction site in the cat ventral pontine tegmentum. *Eur J Neurosci* 6:1829-1836.
- Reynolds ES. 1963. The use of lead citrate at high pH as an electron-opaque stain in electron microscopy. *J Cell Biol* 17:208.
- Roda E, Coccini T, Acerbi D, Castoldi A, Bernocchi G, Manzo L. 2008. Cerebellum cholinergic muscarinic receptor (subtype-2 and -3) and cytoarchitecture after developmental exposure to methylmercury: an immunohistochemical study in rat. *J Chem Neuroanat* 35:285-294. doi: 10.1016/j.jchemneu.2008.01.003.
- Roghani A, Feldman J, Kohan SA, Shirzadi A, Gundersen CB, Brecha N, Edwards RH. 1994. Molecular cloning of a putative vesicular transporter for acetylcholine. *Proc Natl Acad Sci USA* 91:10620-10624.
- Roghani A, Shirzadi A, Kohan SA, Edwards RH, Butcher LL. 1996. Differential distribution of the putative vesicular transporter for acetylcholine in the rat central nervous system. *Mol Brain Res* 43:65-76.
- Roth MT, Fleegal MA, Lydic R, Baghdoyan HA. 1996. Pontine acetylcholine release is regulated by muscarinic autoreceptors. *Neuroreport* 7:3069-3072.
- Rouse ST, Edmunds SM, Yi H, Gilmor ML, Levey AI. 2000. Localization of M(2) muscarinic acetylcholine receptor protein in cholinergic and non-cholinergic terminals in rat hippocampus. *Neurosci Lett* 284:182-186.

- Salgado H, Bellay T, Nichols JA, Bose M, Martinolich L, Perrotti L, Atzori M. 2007. Muscarinic M2 and M1 receptors reduce GABA release by Ca<sup>2+</sup> channel modulation through activation of PI3K/Ca<sup>2+</sup> -independent and PLC/Ca<sup>2+</sup> -dependent PKC. *J Neurophysiol* 98:952-965.
- Seachrist JL, Ferguson SS. 2003. Regulation of G protein-coupled receptor endocytosis and trafficking by Rab GTPases. *Life Sci* 74:225-235.
- Semba K, Reiner PB, Fibiger HC. 1990. Single cholinergic mesopontine tegmental neurons project to both the pontine reticular formation and the thalamus in the rat. *Neuroscience* 38:643-654.
- Shiromani PJ, Fishbein W. 1986. Continuous pontine cholinergic microinfusion via mini-pump induces sustained alterations in rapid eye movement (REM) sleep. *Pharmacol Biochem Behav* 25:1253-1261.
- Shiromani PJ, Winston S, McCarley RW. 1996. Pontine cholinergic neurons show Fos-like immunoreactivity associated with cholinergically induced REM sleep. *Brain Res Mol Brain Res* 38:77-84.
- Steininger TL, Wainer BH, Rye DB. 1997. Ultrastructural study of cholinergic and noncholinergic neurons in the pars compacta of the rat pedunculopontine tegmental nucleus. *J Comp Neurol* 382:285-301.
- Sudhof TC. 2004. The synaptic vesicle cycle. *Annu Rev Neurosci* 27:509-547.
- Swanson LW. 1992. *Structure of the rat brain*. Amsterdam: Elsevier.
- Takata N, Mishima T, Hisatsune C, Nagai T, Ebisui E, Mikoshiba K, Hirase H. 2011. Astrocyte calcium signaling transforms cholinergic modulation to cortical plasticity in vivo. *J Neurosci* 31:18155-18165. doi: 10.1523/JNEUROSCI.5289-11.2011. Erratum in: *J Neurosci* 2012 32:12303.
- Umbriaco D, Watkins KC, Descarries L, Cozzari C, Hartman BK. 1994. Ultrastructural and morphometric features of the acetylcholine innervation in adult rat parietal cortex: an electron microscopic study in serial sections. *J Comp Neurol* 348:351-73.
- Varoqui H, Meunier FM, Meunier FA, Molgo J, Berrard S, Cervini R, Mallet J, Israël M, Diebler MF. 1996. Expression of the vesicular acetylcholine transporter in mammalian cells. *Prog Brain Res* 109:83-95.

- Vilaró MT, Palacios JM, Mengod G. 1994. Multiplicity of muscarinic autoreceptor subtypes? Comparison of the distribution of cholinergic cells and cells containing mRNA for five subtypes of muscarinic receptors in the rat brain. *Mol Brain Res* 21:30-46.
- Vilaró MT, Wiederhold KH, Palacios JM, Mengod G. 1992. Muscarinic M2 receptor mRNA expression and receptor binding in cholinergic and non-cholinergic cells in the rat brain: a correlative study using in situ hybridization histochemistry and receptor autoradiography. *Neuroscience* 47:367-393.
- Wang HL, Morales M. 2009. Pedunculo pontine and laterodorsal tegmental nuclei contain distinct populations of cholinergic, glutamatergic and GABAergic neurons in the rat. *Eur J Neurosci* 29:340-358. doi: 10.1111/j.1460-9568.2008.06576.x.
- Weiner DM, Levey AI, Brann MR. 1990. Expression of muscarinic acetylcholine and dopamine receptor mRNAs in rat basal ganglia. *Proc Natl Acad Sci USA* 87:7050-7054.
- Wess J. 1996. Molecular biology of muscarinic acetylcholine receptors. *Crit Rev Neurobiol* 10:69-99.
- Westerink BH, Enrico P, Feimann J, De Vries JB. 1998. The pharmacology of mesocortical dopamine neurons: a dual-probe microdialysis study in the ventral tegmental area and prefrontal cortex of the rat brain. *J Pharmacol Exp Ther* 285:143-154.
- Westerink BHC, Kwint H-F, De Vries JB. 1996. The pharmacology of mesolimbic dopamine neurons: a dual-probe microdialysis study in the ventral tegmental area and nucleus accumbens of the rat brain. *J Neurosci* 16:2605-2611.
- Williams JA, Reiner PB. 1993. Noradrenaline hyperpolarizes identified rat mesopontine cholinergic neurons in vitro. *J Neurosci* 13:3878-3883.
- Ye M, Hayar A, Strotman B, Garcia-Rill E. 2010. Cholinergic modulation of fast inhibitory and excitatory transmission to pedunculo pontine thalamic projecting neurons. *J Neurophysiol* 103:2417-2432. doi: 10.1152/jn.01143.2009.
- Zhang HM, Chen SR, Pan HL. 2007. Regulation of glutamate release from primary afferents and interneurons in the spinal cord by muscarinic receptor subtypes. *J Neurophysiol* 97:102-109.

Zhang W, Basile AS, Gomeza J, Volpicelli LA, Levey AI, Wess J. 2002. Characterization of central inhibitory muscarinic autoreceptors by the use of muscarinic acetylcholine receptor knock-out mice. *J Neurosci* 22:1709-1717.

Zheng F, Seeger T, Nixdorf-Bergweiler BE, Alzheimer C. 2011. Layer-specific processing of excitatory signals in CA1 interneurons depends on postsynaptic M $\mu$  muscarinic receptors. *Neurosci Lett* 494:217-221. doi: 10.1016/j.neulet.2011.03.016.



## Figure Legend

**Figure 1.** M2 immunolabeling in cholinergic and non-cholinergic neuronal cell bodies.

**A:** A somatodendritic profile (M2-som) identified by Golgi complex cisterns (G) shows some gold particles for M2 (black straight arrows) associated to tubulovesicles (tv) or endoplasmic reticulum (RER) within the cytoplasm, or also attached to the plasma membrane. One M2-immunogold particle is also observed in a small unmyelinated axon in the near neuropil (M2-a). Dense immunoperoxidase precipitate for VAChT (white straight arrows) rims small synaptic vesicles (ssv) within a cholinergic axon terminal (VAChT-t). **B:** An M2-immunoreactive soma (M2-som) shows prominent M2-immunogold particles (black straight arrows) on membranes of tubulovesicles and on the plasma membrane. A dendrite (M2-d) showing prominent gold particles for M2 (black straight arrows) is seen in the adjoining neuropil, where two axon terminals (VAChT-t<sub>1,2</sub>) exhibit immunoperoxidase reaction product for VAChT. **C:** Intense VAChT-immunoperoxidase deposits (white straight arrows) are present on cisterns of the Golgi complex (G) and endomembranes within the cytoplasm in a soma (VAChT+M2-som) showing also M2-immunogold particles (black straight arrows) mainly on the plasma membrane. A M2-labeled dendrite (M2-d) showing immunogold particles for M2 (black straight arrows) is seen in the surrounding neuropil. **D:** A somatodendritic profile (VAChT+M2-som) showing major cytoplasmic distribution for M2-immunogold particles (black straight arrows) also displays more restricted dense VAChT-immunoperoxidase product (white straight arrows) mainly on Golgi cisterns or some adjacent endomembranes. Asterisks, glial profiles. Abbreviation: N, nucleus. Scale bar = 0.5  $\mu$ m in A-D.

**Figure 2.** M2-immunoreactivity in dendrites without VAChT. **A:** Abundant M2-immunogold particles (black straight arrows) are nearly exclusively localized on the plasma membrane of a dendrite (M2-d) making a symmetric synapse (white curved arrow) with an unlabeled terminal (ut<sub>1</sub>) and appositional contacts (white arrowheads) with other unlabeled terminals (ut<sub>2,3</sub>). **B:** A transversely-sectioned large dendrite (M2-d<sub>1</sub>) exhibiting mainly cytoplasmic M2-immunogold particles (black straight arrows) receives multiple contacts from unlabeled terminals (ut<sub>1-3</sub>) whereas a small nearby dendrite (M2-d<sub>2</sub>) showing more obvious plasmalemmal M2-immunogold particles (black straight arrows) unveils no evident contact in the plane of section. Intense immunoperoxidase labeling for VAChT is seen in an adjoining axon terminal (VAChT-t). **C:** Prominent plasmalemmal localization of M2-immunogold particles (black straight arrows) in a dendrite (M2-d) that establishes an apparent symmetric contact (white curved arrow) with an axon terminal (M2-t) having also conspicuous plasmalemmal M2-immunogold (black straight arrows). The inset in the lower left corner shows an enlargement of the contact area illustrating localization of M2-immunogold particle to tubulovesicles attached to the postsynaptic membrane. VAChT-immunoperoxidase product is observed in some small cholinergic axons localized in the near immediacy (VAChT-a<sub>1</sub>) or more distant (VAChT-a<sub>2</sub>) to the M2-immunolabeled profiles. **D:** A longitudinally-sectioned dendrite (M2-d<sub>2</sub>) showing M2-immunogold (black straight arrows) in the cytoplasm forms extensive contact showing multiple synaptic junctions, most of them with unambiguous symmetric morphology (white curved arrow), with an axon terminal (M2-t) containing M2-immunogold particles, some of which are attached to the presynaptic side of the

synapse. The M2- d<sub>2</sub> also received a convergent asymmetric synapse (black curved arrow) from an unlabeled terminal (ut). M2-immunogold (black straight arrows) is also seen mainly associated to tubulovesicles (tv) within a nearby larger dendrite (M2-d<sub>1</sub>) contacting both M2-t and M2-d<sub>2</sub>. Scale bars = 0.5  $\mu$ m in A-D.

**Figure 3.** Bar graph summarizing the mean $\pm$ s.e. immunogold densities (number of gold particles per profile) in M2R-single and VAchT+M2R-dual large (>1 $\mu$ m) or small (<1 $\mu$ m) dendrites within the PPT/LDT. Mean densities were calculated based on the numbers obtained from 1345 VTA dendrites (407 large and 938 small) taken from ultrathin sections from 18 Vibratome sections in 4 rats (2874 total profiles) processed for dual labeling. \*p<0.05, Fisher test for cytoplasmic versus plasmalemmal subcellular localization.

**Figure 4.** M2-immunolabeling in dendrites with VAchT. **A:** A dually labeled large dendrite (VAchT+M2-d) containing M2-immunogold particles (black straight arrows) mostly localized within the cytoplasm attached to vesicular endomembranes (tv) or to a multivesicular body (mvb) and VAchT-immunoperoxidase labeling (white straight arrows) also condensed especially to tv or mvb has large glial ensheathing (asterisks) but also receives input from unlabeled terminals (ut<sub>1,2</sub>), one of which is clearly asymmetric (black curved arrow). **B:** A dendrite (M2- d<sub>1</sub>) showing both VAchT-immunoperoxidase (white straight arrow) and M2-immunogold particles (black straight arrows) makes an asymmetric synapse (black curved arrow) with an unlabeled axon terminal (ut<sub>1</sub>) and a quite more symmetric synapse (white curved arrow) with another

unlabeled axon terminal (ut<sub>2</sub>). Prominent plasmalemmal M2-immunogold particles (black straight arrows) are seen in a near dendrite (M2- d<sub>2</sub>) devoid of VAChT but receiving also input from unlabeled terminals (ut<sub>3,4</sub>). VAChT-immunoperoxidase is also detected in some small unmyelinated axons (VAChT-a<sub>1,2</sub>) in the surrounding area. **C and D:** Serial sections depicting a dual-labeled dendrite (VAChT+M2-d) showing both VAChT-immunoperoxidase (white straight arrows) and M2-immunogold particles (black straight arrows) receives an asymmetric synapse from an axon terminal lightly-labeled for VAChT (VAChT-t). The VAChT+M2-d is close to a longitudinally-sectioned M2-immunogold labeled dendrite (M2- d<sub>1</sub>), but intervening astrocytic leaflet keeps apart from apposition each other profile. Several M2-immugold particles (black straight arrows) are seen in some dendrites (M2- d<sub>2-4</sub>) in one and/or the other of the adjacent serial sections. Abbreviations: asterisks, glial processes. Scale bars = 0.5  $\mu$ m in A-D.

**Figure 5.** VAChT-labeled terminals interactions with M2-labeled profiles. **A:**

Immunoperoxidase reaction product for VAChT rims small synaptic vesicles within a terminal that establishes a symmetric synapse (white curved arrow) onto an M2-immunogold (black straight arrows) labeled dendrite (M2-d). **B:** A transversely-sectioned dendrite (M2-d) showing intracytoplasmic M2-immunogold particles receives convergent input from a VAChT-immunoperoxidase labeled terminal (VAChT-t) and an axon terminal (M2-t) containing numerous M2-immunogold particles. The appositional contact areas of M2-d with both axon terminals (VAChT-t and M2-t) are marked with white arrowheads. **C:** A small VAChT-immunoperoxidase labeled terminal (VAChT-t) contacts an astrocytic profile (M2- g<sub>1</sub>) containing two M2-immunogold particles (black

straight arrows). The M2- g<sub>1</sub> profile makes a gap junction with another glial astrocytic profile (M2- g<sub>2</sub>) that also partially contacts the VAChT-t and shows one M2-immunogold particle in the plane of section. **D**: Axon terminal (VAChT-t<sub>1</sub>) containing VAChT-immunoperoxidase product contacts another terminal (M2-t) showing plasmalemmal M2-immunogold particles (black straight arrows) that makes a symmetric synapse (white curved arrow) with a longitudinally-sectioned M2-labeled dendrite (M2-d). Two smaller intensely VAChT-labeled terminals (VAChT-t<sub>2,3</sub>) and a VAChT-labeled small unmyelinated axon (VAChT-a) are seen in the neighboring neuropil. terminal. Scale bars = 0.5  $\mu$ m in A-D.

**Figure 6.** M2-immunolabeling in axon terminals with VAChT. **A**: Axon terminal containing VAChT-immunoperoxidase mainly on membranes of small synaptic vesicles (VAChT+M2-t) also shows M2-immunogold particles (black straight arrows) and apposes a large dendrite (M2-d) containing intracytoplasmic M2-immunogold. An adjacent axon terminal showing plasmalemmal M2-immunogold makes a symmetric contact (white straight arrow) with an unlabeled dendrite (ud) that receives convergent asymmetric input (black curved arrow) from an unlabeled terminal (ut). **B**: A dually labeled axon terminal (VAChT+M2-t) showing both VAChT-immunoperoxidase and plasmalemmal M2-immunogold particles (black straight arrows) makes a symmetric synapse onto an unlabeled dendrite (ud) receiving convergent asymmetric synaptic input from an unlabeled terminal (ut). A nearby dendrite (M2-d) shows also M2-immunogold labeling on the plasma membrane and tubulovesicular (tv) endomembranes. Scale bars = 0.5  $\mu$ m in A-B.

**Figure 7.** Schematic diagram showing the primary distributions of M2 muscarinic receptors (M2Rs, stars) in neuronal profiles and glial profiles (g) that express (gray filling) or not (white filling) the vesicular acetylcholine transporter (VAChT, black circles) in the rat mesopontine PPT/LDT complex. The M2R is located in a non-VAChT soma (A) whose dendrites receive synaptic inputs from M2R-labeled, VAChT-labeled and/or unlabeled terminals. In these neurons and in VAChT-labeled neurons (B), the M2R is localized mainly to plasma membranes of dendrites, but is also associated with cytoplasmic membranes in both somata and dendrites. These dendrites receive many symmetric (inhibitory-type) and asymmetric (excitatory-type) synapses from terminals that do not contain either M2R or VAChT, both of which are separately located in nearby axonal and glial processes.



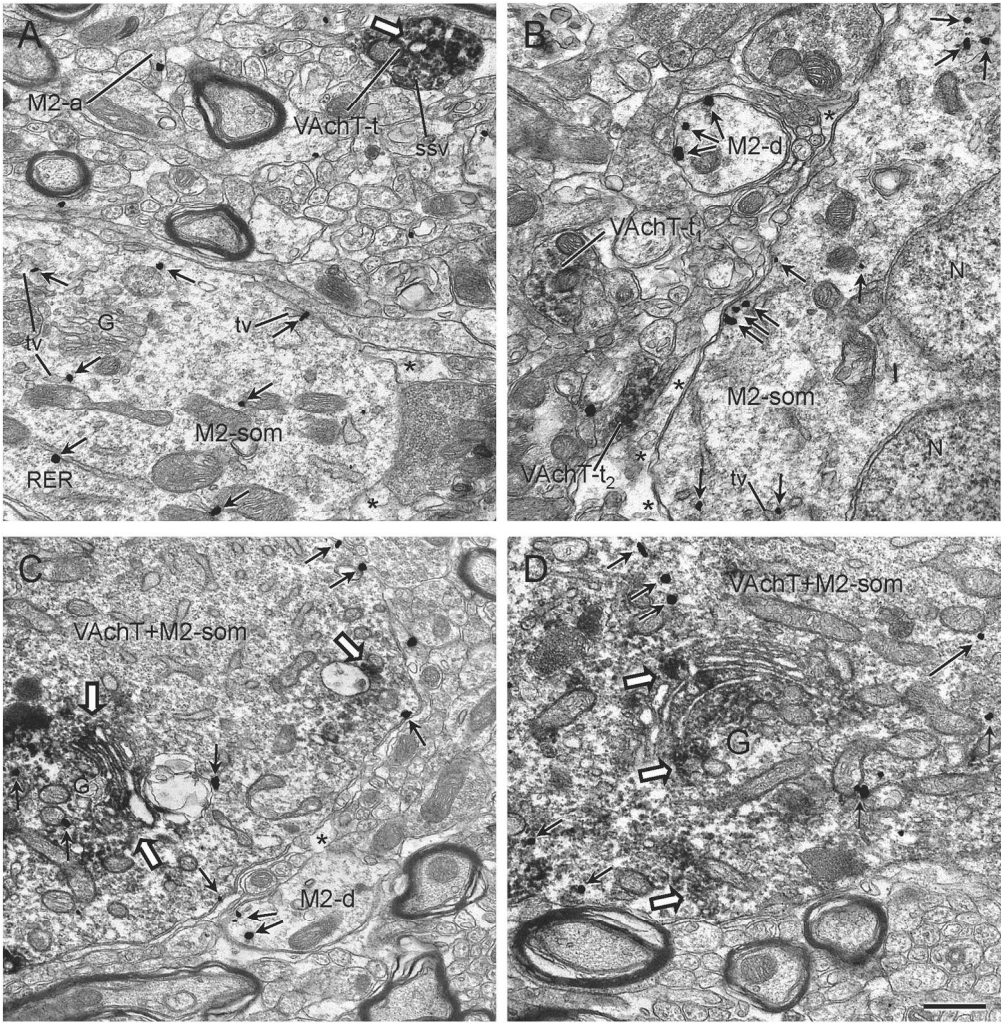


Figure 1. M2 immunolabeling in cholinergic and non-cholinergic neuronal cell bodies. A: A somatodendritic profile (M2-som) identified by Golgi complex cisterns (G) shows some gold particles for M2 (black straight arrows) associated to tubulovesicles (tv) or endoplasmic reticulum (RER) within the cytoplasm, or also attached to the plasma membrane. One M2-immunogold particle is also observed in a small unmyelinated axon in the near neuropil (M2-a). Dense immunoperoxidase precipitate for VAcHT (white straight arrows) rims small synaptic vesicles (ssv) within a cholinergic axon terminal (VAcHT-t). B: An M2-immunoreactive soma (M2-som) shows prominent M2-immunogold particles (black straight arrows) on membranes of tubulovesicles and on the plasma membrane. A dendrite (M2-d) showing prominent gold particles for M2 (black straight arrows) is seen in the adjoining neuropil, where two axon terminals (VAcHT-t1,2) exhibit immunoperoxidase reaction product for VAcHT. C: Intense VAcHT-immunoperoxidase deposits (white straight arrows) are present on cisterns of the Golgi complex (G) and endomembranes within the cytoplasm in a soma (VAcHT+M2-som) showing also M2-immunogold particles (black straight arrows) mainly on the plasma membrane. A M2-labeled dendrite (M2-d) showing immunogold particles for M2 (black straight arrows) is seen in the surrounding neuropil. D: A somatodendritic profile (VAcHT+M2-som) showing major cytoplasmic distribution for M2-immunogold particles (black straight arrows) also displays more restricted dense VAcHT-immunoperoxidase product (white straight arrows) mainly on Golgi cisterns or some adjacent endomembranes. Asterisks, glial profiles. Abbreviation: N, nucleus. Scale bar = 0.5  $\mu$ m in A-D.

171x175mm (300 x 300 DPI)





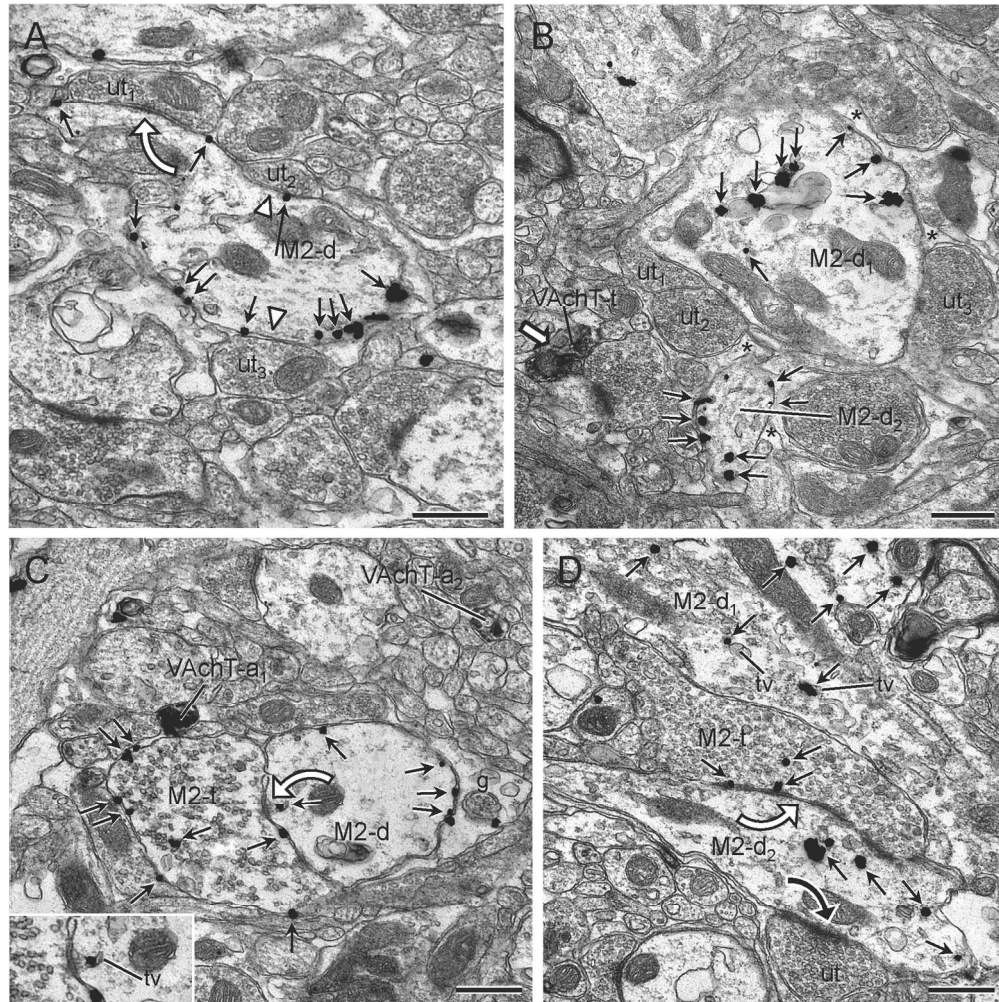


Figure 2. M2-immunoreactivity in dendrites without VAcHT. A: Abundant M2-immunogold particles (black straight arrows) are nearly exclusively localized on the plasma membrane of a dendrite (M2-d) making a symmetric synapse (white curved arrow) with an unlabeled terminal (ut1) and appositional contacts (white arrowheads) with other unlabeled terminals (ut2,3). B: A transversely-sectioned large dendrite (M2-d1) exhibiting mainly cytoplasmic M2-immunogold particles (black straight arrows) receives multiple contacts from unlabeled terminals (ut1-3) whereas a small nearby dendrite (M2-d2) showing more obvious plasmalemmal M2-immunogold particles (black straight arrows) unveils no evident contact in the plane of section. Intense immunoperoxidase labeling for VAcHT is seen in an adjoining axon terminal (VAcHT-t). C: Prominent plasmalemmal localization of M2-immunogold particles (black straight arrows) in a dendrite (M2-d) that establishes an apparent symmetric contact (white curved arrow) with an axon terminal (M2-t) having also conspicuous plasmalemmal M2-immunogold (black straight arrows). The inset in the lower left corner shows an enlargement of the contact area illustrating localization of M2-immunogold particle to tubulovesicles attached to the postsynaptic membrane. VAcHT-immunoperoxidase product is observed in some small cholinergic axons localized in the near immediacy (VAcHT-a1) or more distant (VAcHT-a2) to the M2-immunolabeled profiles. D: A longitudinally-sectioned dendrite (M2-d2) showing M2-immunogold (black straight arrows) in the cytoplasm forms extensive contact showing multiple synaptic junctions, most of them with unambiguous symmetric morphology (white curved arrow), with an axon terminal (M2-t) containing M2-immunogold particles, some of which are attached to the presynaptic side of the synapse. The M2-d2 also received a convergent asymmetric synapse (black curved arrow) from an unlabeled terminal (ut). M2-immunogold (black straight arrows) is also seen mainly associated to tubulovesicles (tv) within a nearby larger dendrite (M2-d1) contacting both M2-t and M2-d2. Scale bars = 0.5  $\mu$ m in A-D.

171x172mm (300 x 300 DPI)

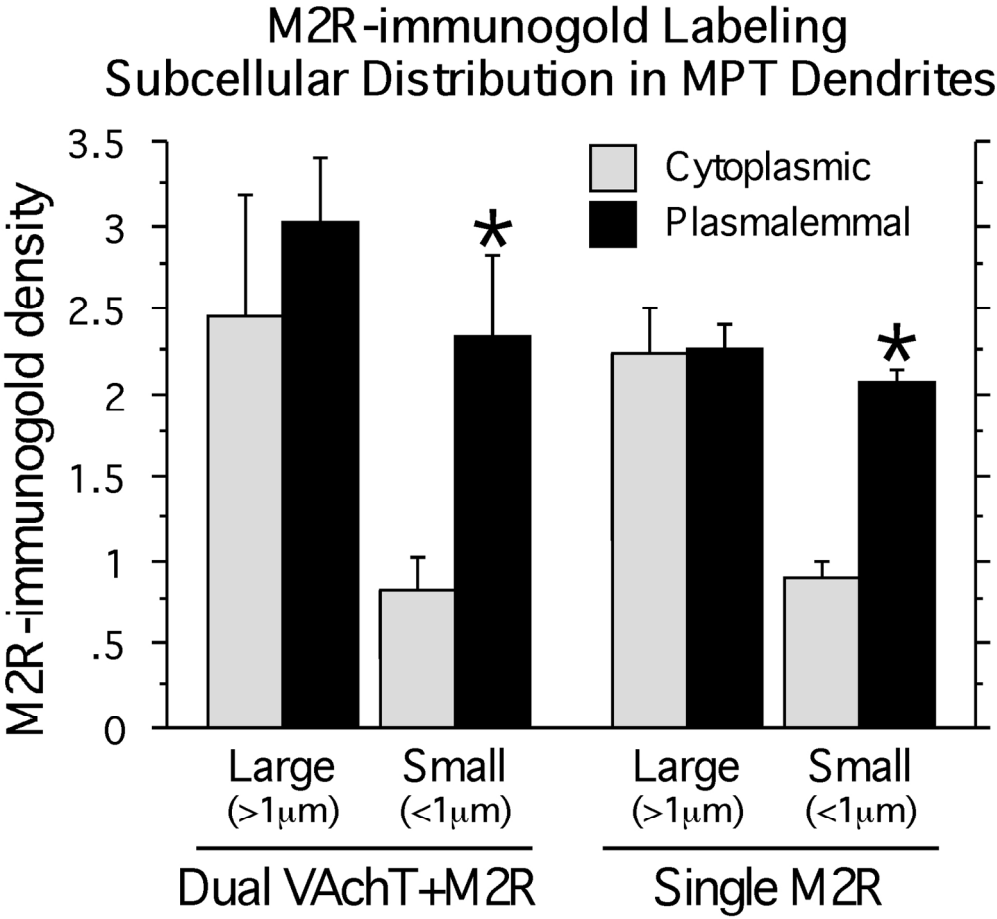


Figure 3. Bar graph summarizing the mean±s.e. immunogold densities (number of gold particles per profile) in M2R-single and VAcHT+M2R-dual large (>1µm) or small (<1µm) dendrites within the PPT/LDT. Mean densities were calculated based on the numbers obtained from 1345 VTA dendrites (407 large and 938 small) taken from ultrathin sections from 18 Vibratome sections in 4 rats (2874 total profiles) processed for dual labeling. \*p<0.05, Fisher test for cytoplasmic versus plasmalemmal subcellular localization.  
80x74mm (600 x 600 DPI)

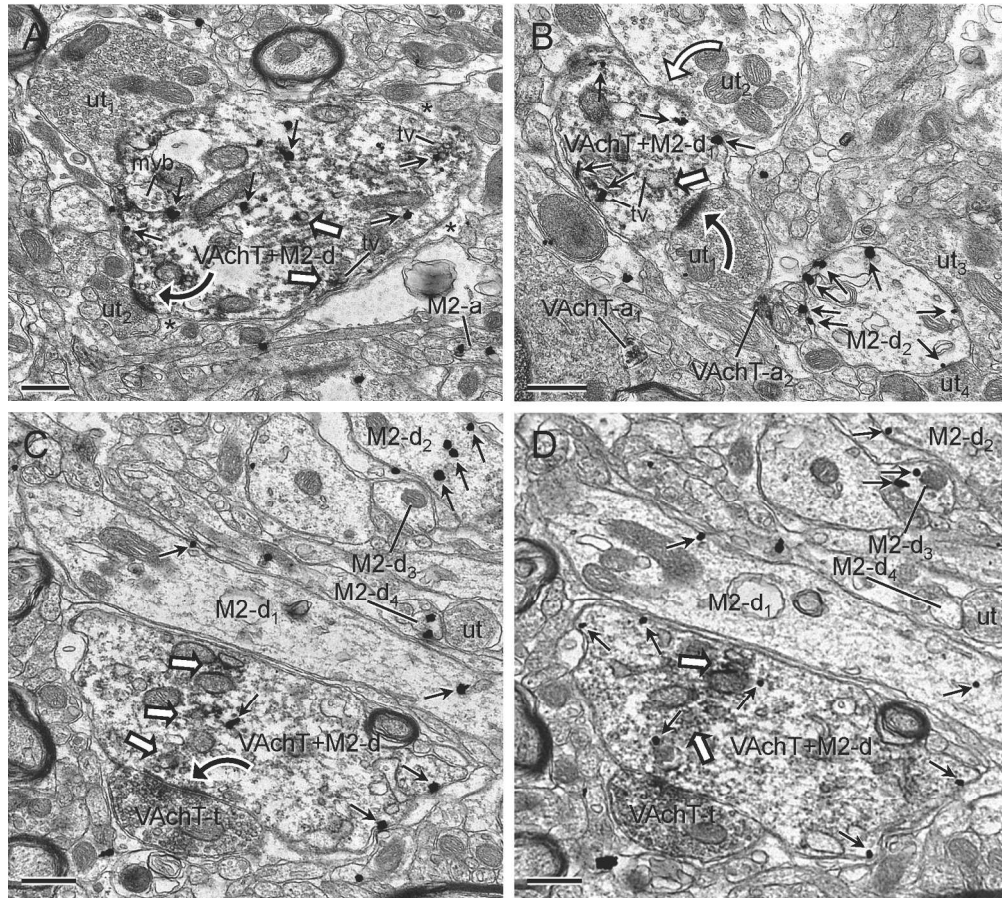


Figure 4. M2-immunolabeling in dendrites with VAcHT. A: A dually labeled large dendrite (VAcHT+M2-d) containing M2-immunogold particles (black straight arrows) mostly localized within the cytoplasm attached to vesicular endomembranes (tv) or to a multivesicular body (mvb) and VAcHT-immunoperoxidase labeling (white straight arrows) also condensed especially to tv or mvb has large glial ensheathing (asterisks) but also receives input from unlabeled terminals (ut<sub>1,2</sub>), one of which is clearly asymmetric (black curved arrow). B: A dendrite (M2- d<sub>1</sub>) showing both VAcHT-immunoperoxidase (white straight arrow) and M2-immunogold particles (black straight arrows) makes an asymmetric synapse (black curved arrow) with an unlabeled axon terminal (ut<sub>1</sub>) and a quite more symmetric synapse (white curved arrow) with another unlabeled axon terminal (ut<sub>2</sub>). Prominent plasmalemmal M2-immunogold particles (black straight arrows) are seen in a near dendrite (M2- d<sub>2</sub>) devoid of VAcHT but receiving also input from unlabeled terminals (ut<sub>3,4</sub>). VAcHT-immunoperoxidase is also detected in some small unmyelinated axons (VAcHT-a<sub>1,2</sub>) in the surrounding area. C and D: Serial sections depicting a dual-labeled dendrite (VAcHT+M2-d) showing both VAcHT-immunoperoxidase (white straight arrows) and M2-immunogold particles (black straight arrows) receives an asymmetric synapse from an axon terminal lightly-labeled for VAcHT (VAcHT-t). The VAcHT+M2-d is close to a longitudinally-sectioned M2-immunogold labeled dendrite (M2- d<sub>1</sub>), but intervening astrocytic leaflet keeps apart from apposition each other profile. Several M2-immugold particles (black straight arrows) are seen in some dendrites (M2- d<sub>2-4</sub>) in one and/or the other of the adjacent serial sections. Abbreviations: asterisks, glial processes. Scale bars = 0.5  $\mu$ m in A-D.  
172x153mm (306 x 306 DPI)

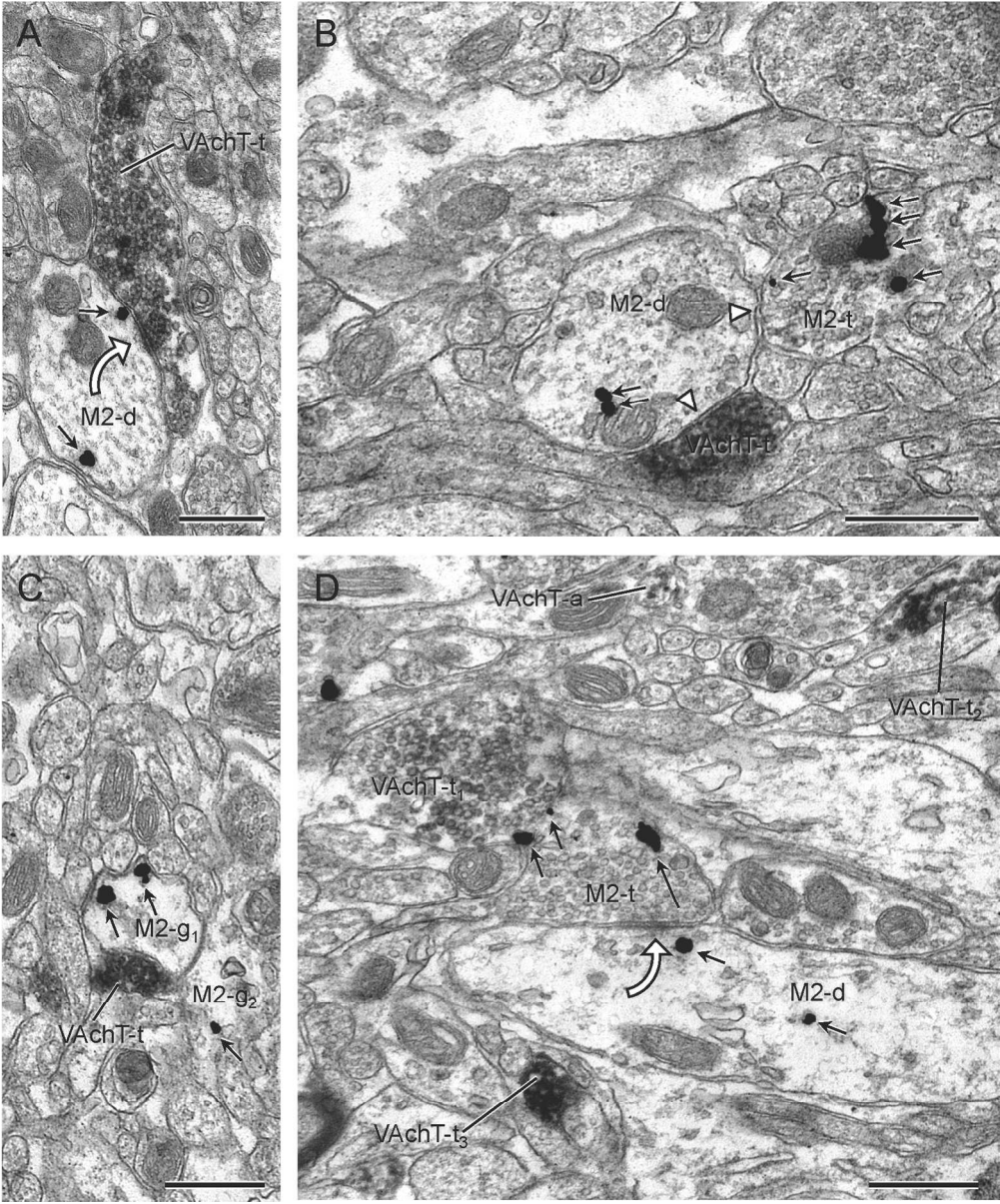


Figure 5. VAcHT-labeled terminals interactions with M2-labeled profiles. A: Immunoperoxidase reaction product for VAcHT rims small synaptic vesicles within a terminal that establishes a symmetric synapse (white curved arrow) onto an M2-immunogold (black straight arrows) labeled dendrite (M2-d). B: A transversely-sectioned dendrite (M2-d) showing intracytoplasmic M2-immunogold particles receives convergent input from a VAcHT-immunoperoxidase labeled terminal (VAcHT-t) and an axon terminal (M2-t) containing numerous M2-immunogold particles. The appositional contact areas of M2-d with both axon terminals (VAcHT-t and M2-t) are marked with white arrowheads. C: A small VAcHT-immunoperoxidase labeled terminal (VAcHT-t) contacts an astrocytic profile (M2- g<sub>1</sub>) containing two M2-immunogold particles (black straight arrows). The M2- g<sub>1</sub> profile makes a gap junction with another glial astrocytic profile (M2- g<sub>2</sub>) that also partially contacts the VAcHT-t and shows one M2-immunogold particle in the plane of section. D: Axon terminal (VAcHT-t<sub>1</sub>) containing VAcHT-immunoperoxidase product contacts another terminal (M2-t) showing plasmalemmal M2-immunogold particles (black straight arrows) that makes a symmetric synapse (white curved arrow) with a longitudinally-sectioned M2-labeled dendrite (M2-d). Two smaller intensely VAcHT-

labeled terminals (VAChT-t2,3) and a VAChT-labeled small unmyelinated axon (VAChT-a) are seen in the neighboring neuropil. terminal. Scale bars = 0.5  $\mu$ m in A-D.  
171x206mm (300 x 300 DPI)

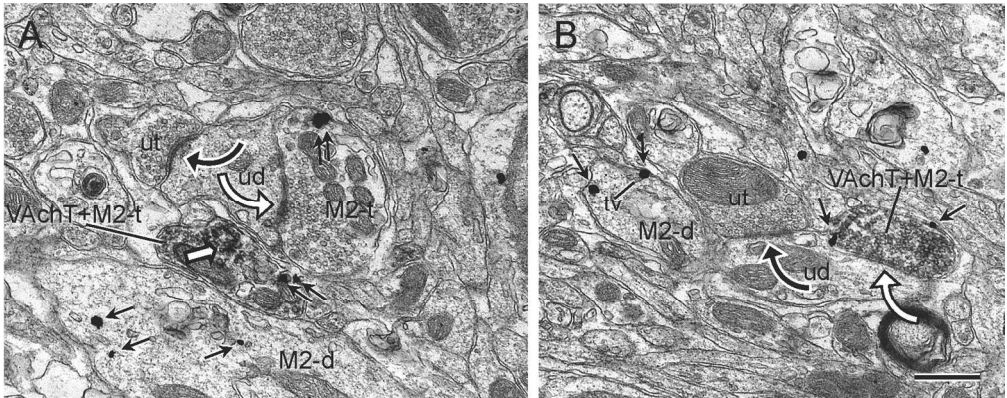


Figure 6. M2-immunolabeling in axon terminals with VAChT. A: Axon terminal containing VAChT-immunoperoxidase mainly on membranes of small synaptic vesicles (VAcHT+M2-t) also shows M2-immunogold particles (black straight arrows) and apposes a large dendrite (M2-d) containing intracytoplasmic M2-immunogold. An adjacent axon terminal showing plasmalemmal M2-immunogold makes a symmetric contact (white straight arrow) with an unlabeled dendrite (ud) that receives convergent asymmetric input (black curved arrow) from an unlabeled terminal (ut). B: A dually labeled axon terminal (VAcHT+M2-t) showing both VAChT-immunoperoxidase and plasmalemmal M2-immunogold particles (black straight arrows) makes a symmetric synapse onto an unlabeled dendrite (ud) receiving convergent asymmetric synaptic input from an unlabeled terminal (ut). A nearby dendrite (M2-d) shows also M2-immunogold labeling on the plasma membrane and tubulovesicular (tv) endomembranes. Scale bars = 0.5  $\mu\text{m}$  in A-B.

171x67mm (300 x 300 DPI)



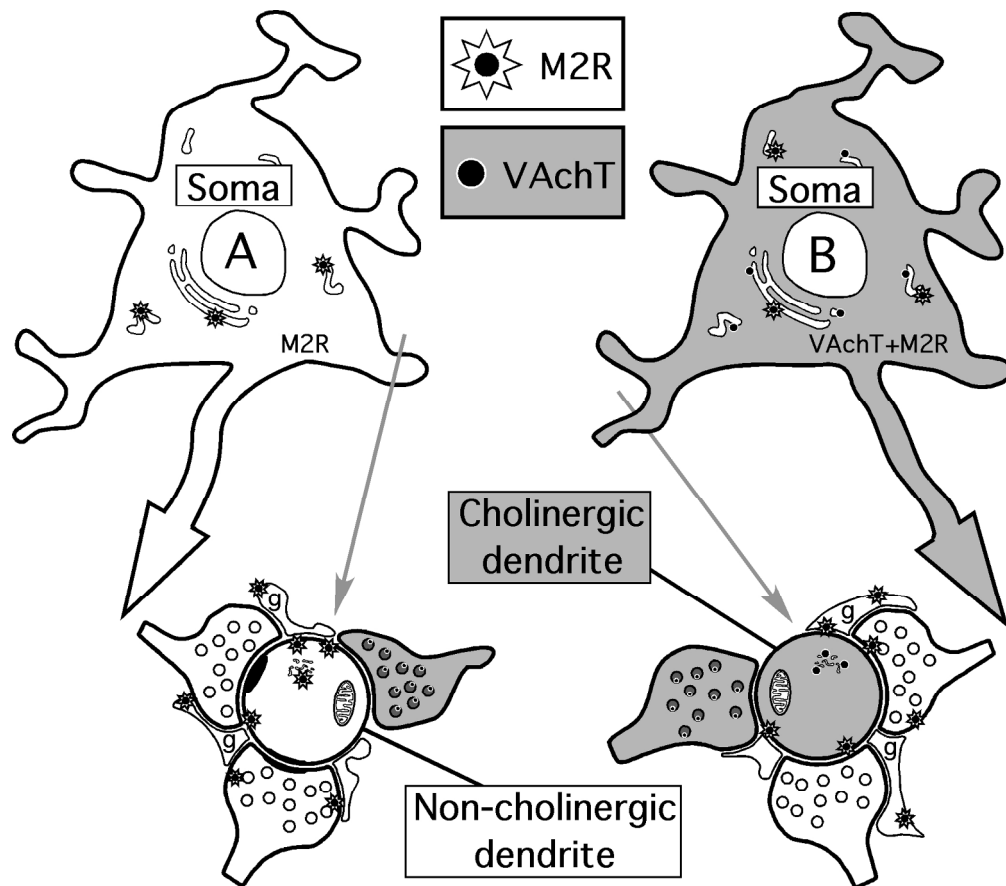


Figure 7. Schematic diagram showing the primary distributions of M2 muscarinic receptors (M2Rs, stars) in neuronal profiles and glial profiles (g) that express (gray filling) or not (white filling) the vesicular acetylcholine transporter (VAChT, black circles) in the rat mesopontine PPT/LDT complex. The M2R is located in a non-VAChT soma (A) whose dendrites receive synaptic inputs from M2R-labeled, VAChT-labeled and/or unlabeled terminals. In these neurons and in VAChT-labeled neurons (B), the M2R is localized mainly to plasma membranes of dendrites, but is also associated with cytoplasmic membranes in both somata and dendrites. These dendrites receive many symmetric (inhibitory-type) and asymmetric (excitatory-type) synapses from terminals that do not contain either M2R or VAChT, both of which are separately located in nearby axonal and glial processes.

175x153mm (300 x 300 DPI)

**Table 1.** Primary Antibodies Used

Antigen	Immunogen	Manufacturer	Dilution
M2R	Synthetic fusion protein containing glutathione S-transferase fused to a part of the i3 intracellular loop of human M2R (residues 225-356)	Alomone Labs Ltd (AMR-002 [lot AN-08]) RRID: AB_2039995 Rabbit polyclonal	1:100 (gold)  1:2000 (peroxidase)
VAchT	20 residue C-terminal synthetic peptide sequence corresponding to amino acids 511-530 of the cloned rat VAchT	ImmunoStar (cat. 24286) RRID: AB_572269 Goat polyclonal	1:16000 (peroxidase)  1:3000 (gold)

VAchT, vesicular acetylcholine transporter; M2R, M2 muscarinic receptor.

**Table 2.** Neuronal distribution of M2 and/or VAChT immunolabeled cellular profiles in the rat mesopontine PPT/LDT

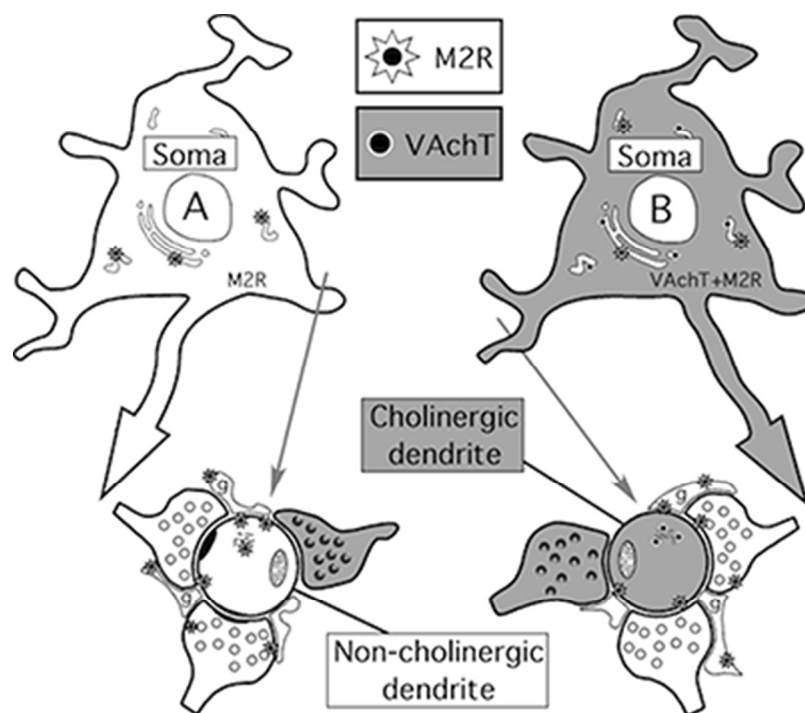
TYPE OF CELLULAR PROFILE	LABELING								
	Total M2	Single M2		Dual VAChT+M2		Single VAChT		Total VAChT	
	Number of profiles	% from total M2	Number of profiles	% from total M2	Number of profiles	% from total VAChT	Number of profiles	% from total VAChT	Number of profiles
Dendrites	1345	84.2	1133	15.8	212	43.4	276	56.6	488
Somata	42	64.3	27	35.7	15	93.8	1	6.2	16
Axon Terminals	199	94.5	188	5.5	11	2.5	424	97.5	435
Unmyelinated Axons	254	98.4	250	1.6	4	1.5	266	98.5	270
Myelinated Axons	14	71.4	10	28.6	4	44.4	5	55.6	9
Glia	46	100	46	0	0	0	2	100	2
TOTAL	1900	87.1	1654	12.9	246	20.2	974	79.8	1220

Immunolabelings for M2 and/or VAChT in different neuronal compartments within the rat PPT/LDT. Profiles containing single M2-, single VAChT- and dual VAChT+M2-labelings are given as raw numbers and as percentage of the total M2 and/or total VAChT immunolabeled profiles in each category. Data were collected from 18 Vibratome sections in 4 rats processed for dual labeling. Labeling in profiles not clearly distinguished as neuronal or glial is not included in the table.

**Table 3** Numbers of Asymmetric and Symmetric axodendritic synapses having VAchT- and/or M2R- immunoreactivity at pre- and/or post-synaptic sites within the rat mesopontine PPT and LDT nuclei.

Presynaptic terminals	Postsynaptic dendrites							
	M2R		VAchT+M2R		VAchT		Unlabeled	
	Asym	Sym	Asym	Sym	Asym	Sym	Asym	Sym
M2R	10	15	7	1	0	1	13	23
Dual (VAchT+M2R)	2	1	0	0	0	0	0	0
VAchT	14	15	1	2	2	2	7	15
Unlabeled	235	259	38	12	16	63	---	---
TOTAL	261	290	46	15	18	66	20	38

Total numbers of asymmetric (Asym) and symmetric (Sym) synapses containing single M2-, single VAchT- and dual VAchT+M2R-at pre- and/or post- synaptic sites in axodendritic synapses within the PPT/LDT are given as raw numbers in each category. Data were collected from 18 Vibratome sections in 4 rats processed for dual labeling.



141x123mm (72 x 72 DPI)

Muscarinic M2 receptors are identified mainly on plasma membranes and endomembranes of cholinergic and non-cholinergic neurons and rarely on axonal and glial processes in the mesopontine tegmentum. This has important implications for intracellular M2R trafficking and M2-mediated control of sleep-wake cycle through autoreceptors and heteroreceptors in this brain region.